coatings

MDPI

Article

Polyacrylate Latex Coating Binders Comprising Polypyrrole Component Prepared with "One-Pot" Synthesis

Karolína Boštíková [1,*], Miroslav Kohl [1], Andréa Kalendová [1], Petr Knotek [2], Miroslava Trchová [3], Jaroslav Stejskal [4], Eva Schmidová [5] and Jana Machotová [1]

1 Institute of Chemistry and Technology of Macromolecular Materials, Faculty of Chemical Technology, University of Pardubice, Studentská 573, 532 10 Pardubice, Czech Republic; miroslav.kohl@upce.cz (M.K.); andrea.kalendova@upce.cz (A.K.); jana.machotova@upce.cz (J.M.)
2 Department of General and Inorganic Chemistry, Faculty of Chemical Technology, University of Pardubice, Studentská 573, 532 10 Pardubice, Czech Republic; petr.knotek@upce.cz
3 Central Laboratories, University of Chemistry and Technology, 166 28 Prague, Czech Republic; miroslava.trchova@vscht.cz
4 University Institute, Tomas Bata University in Zlín, 760 01 Zlín, Czech Republic; stejskal@utb.cz
5 Jan Perner Transport Faculty, Educational and Research Centre in Transport, University of Pardubice, 533 53 Pardubice, Czech Republic; eva.schmidova@upce.cz
* Correspondence: karolina.bostikova@student.upce.cz; Tel.: +420-446-037-329

Abstract: This work deals with the coating properties of synthetic latices comprising two kinds of polymers, specifically polyacrylate and polypyrrole, which were simultaneously formed by semi-continuous emulsion polymerization using a "one-pot" synthesis strategy. In this procedure, both the emulsion polymerization of acrylate monomers and the oxidative polymerization of pyrrole occurred concurrently in one reactor. Polyacrylate latices differing in polypyrrole loading were prepared by applying various dosages of pyrrole, specifically 0, 0.25, and 0.50, based on the fraction of acrylate monomers. The effect of the in situ incorporated polypyrrole component (having the nature of submicron composite polypyrrole-coated polyacrylate latex particles) on the physico-mechanical properties and chemical resistance of the resulting heterogeneous coating films was investigated. The interaction of incorporated polypyrrole and anti-corrosion pigments (see ZnS, $Zn_3(PO_4)_2$, $ZnFe_2O_4$, MoS_2, and ZnO) on the corrosion resistance of coatings was evaluated by using the electrochemical linear polarization technique. The polyacrylate latex prepared with the lowest polypyrrole loading (achieved by polymerizing 0.25 wt. % of pyrrole related to acrylic monomers) was found to be the optimum binder for waterborne anticorrosive coatings based on their properties and protective function. Their compatibility with the selected types of pigments was studied for these latex binders. In addition, their influence on the anti-corrosion efficiency of polyacrylate paint films was evaluated using the linear polarization electrochemical technique. For high corrosion resistance, the ZnS and MoS_2 pigments, showing compatibility with polyacrylate latices containing the polypyrrole component, proved to be advantageous.

Keywords: emulsion polymerization; polyacrylate latex; polypyrrole; anti-corrosion coating; corrosion resistance; electrochemical linear polarization

Citation: Boštíková, K.; Kohl, M.; Kalendová, A.; Knotek, P.; Trchová, M.; Stejskal, J.; Schmidová, E.; Machotová, J. Polyacrylate Latex Coating Binders Comprising Polypyrrole Component Prepared with "One-Pot" Synthesis. *Coatings* **2024**, *14*, 1565. https://doi.org/10.3390/coatings14121565

Academic Editor: Alin Dinita

Received: 5 November 2024
Revised: 8 December 2024
Accepted: 9 December 2024
Published: 13 December 2024

1. Introduction

Two of the most important challenges in coating technology and manufacturing are the development of safer products and safer processes and the reduction of solvent emissions in the air, with zero emissions being one of the most significant achievements [1–4]. Organic vapors released from solvent-based industrial coatings are important precursors of secondary organic aerosols which threaten human health and the environment. For solvent-based paints, the volatile (VOC) and medium-volatile organic compound (IVOC) emission factors are 129–254 and 25–80 g/kg, respectively, while for water-based paints, VOC and

IVOC values are about 32 and 13 g/kg, respectively [5,6]. For these reasons, synthetic latices, specifically waterborne dispersions of submicron polymer particles produced by emulsion polymerization technology, are receiving considerable attention nowadays and are often used as binders of environmentally friendly paints [7–10]. Among the common latex paint binders, polyacrylate latices and their coating films are appreciated for their excellent resistance to weathering and UV radiation, transparency, chemical resistance, and adhesion to various substrates [11–13]. Moreover, polyacrylates do not usually react with pigments or fillers, enabling their easy dispersion in the latex binder [14].

In the case of anti-corrosion pigmented coatings, the requirements for safer products are mainly ensured by the complete removal of chromium- and lead-based pigments [15]. The application of conductive polymers, including polypyrrole, appears to be a possibility to replace these toxic anti-corrosion pigments. Polypyrrole has gained special attention not only for its intrinsic conductivity but also for its good environmental stability, ease of preparation, and availability of a starting pyrrole monomer [16–19]. Polypyrrole can be synthesized by oxidative polymerization in the form of a polycation with delocalized charges [20]. To maintain electroneutrality, the anions present compensate for the delocalized charges on the polymer chain [19,21–26]. The resulting conductivity of polypyrrole depends on the synthesis conditions and reactants, such as the choice in oxidizing agent, solvent, co-dopant, reaction temperature, pyrrole, and surfactant concentrations. Among the solvents, water has been reported as the most convenient one concerning the required conductivity characteristics [27,28]. Among the oxidizing agents, ferric chlorate, ferric chloride, and ammonium peroxodisulfate are typically utilized, with the latter being found to provide the best intrinsic electrical conductivity of polypyrrole [19,29]. A severe drawback of polypyrrole is its rigid nature, caused by strong intramolecular and intermolecular interactions, which causes insolubility in common solvents and thus the incapability of dispersion in organic paints [29,30].

To facilitate polypyrrole processability and utilization, oxidative polymerization of pyrrole performed in emulsion polymerization mode has been investigated as a promising method of providing submicron polypyrrole particles. Research in this area was mainly focused on the influence of the surfactant type on the conductivity of the prepared nanosized polypyrrole, wherein peroxodisulfate oxidizing agents [19,31] and anionic surfactants (e.g., sodium dodecyl sulfate (SDS)) have been proven to be particularly effective [19,31–33]. Furthermore, the control of polypyrrole's particle size and morphology via operational conditions in emulsion polymerization was studied, and it was found that nanosized polypyrrole with uniform morphology and relatively high conductivity was obtained using a semi-continuous feeding system [33].

Nevertheless, the application of polypyrrole in latex protective coatings has been rarely reported. The only reports on systems based on polypyrrole-coated film-forming latices in which the latex substrate was based on styrene-butadiene rubber [26], polyurethane [34], or polyacrylate [35] were found in the relevant literature without focusing on the anti-corrosion efficiency of the coatings. In all of these cases, polypyrrole-coated conductive composite core-shell latex particles were prepared via in situ oxidative polymerization of pyrrole in aqueous media containing film-forming latex particles which had been synthesized by a standard process of emulsion polymerization. However, this strategy lacks practical application on the industrial scale because of high latex dilution (about 5 wt. % of solids) or the need for latex purification via repeated centrifugation-redispersion cycles to remove the unwanted inorganic byproducts produced during pyrrole polymerization. To the best of our knowledge, no reports on the oxidative polymerization of pyrrole occurring simultaneously in a single reactor during the synthesis of a film-forming latex via emulsion polymerization have been presented. Moreover, information on the anti-corrosion effect of polypyrrole incorporated in any way into latex coatings is scarce. Both of these facts have motivated the present work.

In this paper, heterogeneous film-forming polyacrylate latices in which two kinds of polymers, specifically polyacrylate and polypyrrole, were prepared using a simple "one-

pot" synthesis strategy, where both the emulsion polymerization of acrylate monomers and the oxidative polymerization of pyrrole occurred together in a single reactor. Polyacrylate latices varying in polypyrrole loading (provided by 0–0.5 wt. % pyrrole based on the acrylate monomers fraction) were synthesized. The chemical structure of the polypyrrole synthesized during emulsion polymerization and the storage stability of the latices were evaluated. The anti-corrosion effect of the incorporated polypyrrole component in combination with various pigments was studied using the electrochemical linear polarization technique and cyclic corrosion tests in a salt mist atmosphere.

2. Materials and Methods

2.1. Materials

The latices were prepared from methyl methacrylate (MMA), butyl acrylate (BA), and methacrylic acid (MAA). Sigma Aldrich (Prague, Czech Republic) supplied these monomers and the pyrrole. The emulsifier used was Disponil FES 993 (anionic surfactant based on polyglycol ether sulfate; BASF, Chrudim, Czech Republic). Ammonium peroxodisulfate (Lach-Ner Ltd., Neratovice, Czech Republic) was the initiator and, at the same time, the oxidizing agent. Dehydran® 1239 (mixture of modified polysiloxanes; Henkel, Düsseldorf, Germany) was used as the defoamer.

2.2. Pigments

The pigments were zinc oxide (ZnO; Sigma Aldrich Prague branch), zinc phosphate ($Zn_3(PO_4)_2$; Heubach GmbH, Langelsheim, Germany), zinc sulfide (ZnS; Sigma Aldrich, Prague branch, Czech Republic), zinc ferrite ($ZnFe_2O_4$; laboratory synthesis at the University of Pardubice) and molybdenum disulfide (MoS_2, Sigma Aldrich, Prague Branch, Czech Republic).

2.3. Synthesis

The polyacrylate latices with different polypyrrole loadings were prepared by polymerizing various pyrrole dosages, namely 0, 0.25, and 0.5 wt. %, based on the fraction of acrylate monomers during the synthesis of polyacrylate latex binder under a "one-pot" synthesis strategy. In this method, both the emulsion radical polymerization of acrylate monomers and the oxidative polymerization of pyrrole occurred simultaneously in one reactor. Ammonium peroxodisulfate was used as both the initiator for the radical polymerization of acrylates and the oxidizing agent for the oxidative polymerization of pyrrole. MMA, BA, and MAA were used as the initial monomers at a 45/51/44 mass ratio to synthesize the polyacrylate polymer.

Latices were prepared in a stirred reaction vessel at a polymerization temperature of 85 °C under an inert nitrogen atmosphere. Distilled water and the emulsifier were introduced into the reaction vessel (Table 1). Simultaneously, the first emulsion of the acrylate monomers was prepared in an emulsification flask by mixing the components (distilled water, initiator, emulsifier, MMA, BA, and MAA). After the reaction vessel charge was heated to the polymerization temperature, the proportion of the initiator intended for the reaction vessel mixture was added to the reaction vessel. Then, the first acrylate monomer emulsion was dosed dropwise for 60 min. Later, the reaction mixture was maintained at 85 °C for 15 min. Concurrently, the second emulsion of the acrylate monomers (distilled water, initiator, emulsifier, MMA, BA, and MAA) was prepared in an emulsification flask. For the latices designed to contain the polypyrrole component, a pyrrole solution (distilled water and pyrrole) was prepared in parallel by mixing both components in a controlled-flow flask. The second acrylate monomer emulsion and pyrrole solution were then dosed simultaneously dropwise to the reaction vessel for an additional 60 min. Subsequently, the reaction mixture was maintained at 85 °C for 120 min to complete the polymerization process. The reaction vessel containing the resulting latex was then cooled under constant stirring in an inert atmosphere to 25 °C. Half of the latex was used as prepared, and in the following text, it is referred to as acidic latex ($L_{acid\_polypyrrole\ loading\ (wt.\ \%)}$). The other half

of the latex was alkalized with a 10% aqueous ammonia solution to pH = 8.5, and in the following text, this latex is referred to as alkaline latex ($L_{alkali\_polypyrrole\ loading\ (wt.\ \%)}$).

Table 1. Composition of the reaction mixtures for synthesizing polyacrylate latices with different polypyrrole loadings.

	Pyrrole Dosage [a] (wt. %)		
	0	**0.25**	**0.50**
Reaction Vessel			
Distilled water (g)	75.0	75.0	75.0
Disponil FES 99 (g)	0.5	0.5	0.5
Ammonium peroxodisulfate (g)	0.4	0.4	0.4
The First Monomer Emulsion			
Distilled water (g)	75.0	75.0	75.0
Disponil FES 99 (g)	7.3	7.3	7.3
MMA (g)	45.0	45.0	45.0
BA (g)	51.0	51.0	51.0
MAA (g)	4.0	4.0	4.0
Ammonium peroxodisulfate (g)	0.4	0.4	0.4
The Second Monomer Emulsion			
Distilled water (g)	155.0	155.0	155.0
Disponil FES 99 (g)	7.3	7.3	7.3
MMA (g)	45.0	45.0	45.0
BA (g)	51.0	51.0	51.0
MAA (g)	4.0	4.0	4.0
Ammonium peroxodisulfate (g)	0.4	1.9	4.0
Pyrrole Solution			
Pyrrole (g)	0	0.5	1.0
Distilled water (g)	-	65.0	65.0

[a] Based on the total mass of acrylate monomers used in the polymerization system.

2.4. Characterization of Latices

The content of the coagulum was determined according to standard CSN 64 9008 [36] through sieve analysis [37]. The content of solids was determined according to EN ISO 3251 [38]. For the determination of the conversion [39] immediately after completion of the latex synthesis, 1 ± 0.2 g of latex was weighed on an analytical balance in a Petri dish. The procedure was repeated three times for each latex sample in these determinations, and the resulting value was calculated as the arithmetic mean. The pH measurements were carried out according to protocol ISO 787-9 [40] at 23 ± 1 °C using a FiveEasy FE20 pH meter (Mettler-Toledo; Greifensee, Switzerland) [41]. The minimum film-forming temperature (MFFT) was determined according to standard ISO 2115 [42] using an MFFT-60 device (Rhopoint Instruments; Hastings, UK) [43]. The glass transition temperature (T_g) was determined by differential scanning calorimetry (DSC) with a Pyris 1 DSC instrument (Perkin-Elmer; Waltham, MA, USA). The measurements were performed under an inert (nitrogen) atmosphere at a heating rate of 10 °C/min from −50 °C to 120 °C.

2.5. Spectroscopic Analysis of Polypyrrole

The molecular structure of the polypyrrole synthesized during emulsion polymerization was studied using Fourier transform infrared (FTIR) spectroscopy with a Thermo Nicolet NEXUS 870 FTIR spectrometer with a DTGS TEC detector (ThermoFisher Scientific; Waltham, MA, USA) in the range of 400–4000 cm^{-1}. Analyses of the synthesized polypyrrole and Disponil FES 993 emulsifier were provided through the ATR technique, and reference powder samples of the polypyrrole salt and deprotonated polypyrrole base were dispersed in potassium bromide pellets for analysis. The polypyrrole for the spectroscopic analysis was prepared using the same "one-pot" procedure and components described above for the polyacrylate latex with a pyrrole dosage of 0.5 wt. %, except no

acrylate monomers were introduced into the polymerization system. The above substances were also analyzed using Raman spectroscopy. Raman spectra excited by the HeNe 633 nm laser were obtained using a Renishaw inVia Reflex Raman microspectrometer (Renishaw, England) with a Peltier-cooled CCD detector (576 × 384 pixels).

2.6. Determination of Stability of Latices

The storage stability of the synthesized latices was tested after one month and four months of storage in an oven at 40 °C. The evaluation was performed visually, and after removal of the sample from the oven, the color change, coagulum formation, and latex precipitation were evaluated. The stability of the prepared latices against electrolytes was monitored, depending on the type of electrolyte and the chosen electrolyte concentration (0.32, 0.63, 1.25, 2.5, or 5 $g \cdot L^{-1}$). Stability testing was performed with three different electrolytes, namely NaCl, $CaCl_2$, and $FeCl_3$ [44]. The evaluation was performed visually to determine whether precipitation of the dispersion occurred. The average particle size and zeta potential were used to evaluate the colloidal stability of the freshly prepared latices [45]. The average particle size and zeta potential of the latex particles dispersed in the aqueous phase were detected immediately after the latex synthesis via dynamic light scattering using a Litesizer 500 (Anton Paar GmbH; Graz, Austria). The concentration of the solid polymer in the aqueous phase was 0.01 wt. %, and the measurements were performed at 25 °C [46].

2.7. Morphology of Coatings

The polyacrylate latex coating films were monitored by scanning electron microscopy (SEM). To test latex films containing different polypyrrole loading, free-standing films were prepared by casting and drying the latices in silicone molds at 23 ± 2 °C and at a relative humidity of 50 ± 5%. The topography of the coating film was monitored on the fracture surface, which was prepared in a liquid N_2 environment. The sample was first coated with a 20–25 nm-thick gold layer using an SCD 050 (Balzers) and then observed in secondary electron mode using a LYRA 3 scanning electron microscope (Tescan, Brno, Czech Republic) [47]. Elemental analysis of polyacrylate latex coating films containing different polypyrrole loading was performed with a Flash 2000 CHNS Elemental Analyzer (Thermo Fisher Scientific, Milan, Italy). The surface mechanical homogeneity of the coating films was evaluated by employing atomic force microscopy (AFM) in the mode of the PeakForce quantitative nanoscale mechanics (PF-QNM). Measurements were achieved by applying a Dimension Icon AFM (Bruker, Billerica, MA, USA) using ScanAsyst-Air tips (k = 0.4 $N \cdot m^{-1}$) and a 512 × 512 pixel resolution. For details on data acquisition and processing, see [48,49].

2.8. Determination of Physicochemical Properties of Inorganic Pigments

The inorganic pigments were characterized using parameters important for application in paints, such as density (determined by Micromeritics AutoPycnometer 1340 (Norcross, GA, USA)) and oil absorption (determined by the "pestle–mortar" method). Based on these determined parameters, the critical pigment volume concentrations (CPVCs) of the individual studied pigments were calculated [50,51].

2.9. Preparation of Pigmented Coatings

The latices were combined with pigments (ZnO, $ZnFe_2O_4$, ZnS, MoS_2, and $Zn_3(PO_4)_2$) at a concentration of 8 wt. % (based on the latex fraction). Their effect on the protective properties of latex binders or the increase in anticorrosive effectiveness of the pigmented coatings was tested. The dispersion was carried out on a Disolver-type apparatus (Dispermat CN30-F2, VMA-Getzmann GMBH; Reichshol, Germany) using 2.8 mm-diameter beads at a speed of 1500 rpm for 30 min, resulting in uniform dispersion of the pigment in the latex binder. After dispersion, the prepared waterborne paints were filtered and stored in glass containers.

2.10. Preparation of Paint Film Samples for Testing

The test coatings were created using a set of applicators (Zehntner GmbH Testing Instruments; Sissach, Switzerland) with slit sizes of 150, 200, and 250 µm at 23 ± 2 °C and a relative humidity of 50 ± 5% according to ISO 1514 [52]. The samples for the physical-mechanical and electrochemical tests were prepared in one pass, targeting DFT = 60 µm. In contrast, the samples for the cyclic corrosion test were prepared in two passes, targeting DFT = 100 µm. Before starting the tests, the coatings on the test panels were left to dry in a climate-controlled room under the same conditions for 30 days [53]. After drying, the dry film thickness (DFT) of the coatings was measured using a three-point thickness gauge (Schut-20, Schut Geometrische Meettechniek BV; Groningen, the Netherlands) for coatings applied on glass panels and a magnetic thickness gauge (Byko-test 8500 premium Fe/Nfe, BYK Additives & Instruments; Wesel, Germany) for those on steel panels according to EN ISO 2808 [54]. The prepared latices were applied to glass and steel panels (Q-Lab Corporation; Cleveland, OH, USA). The ZQD-SP-104171 panel type was utilized for mechanical testing, the QD-24 panel type was used for the electrochemical linear polarization technique, and the S-46 panel type was used for the cyclic corrosion test. The characterization of the steel panels used is summarized in Table 2.

Table 2. Characterization of used steel panels.

Panel Type	Dimensions (mm)	Roughness (µm)	Chemical Composition (%)
S46	152 × 102 × 0.81	0.5–1.15	Mn ≤ 0.60 C ≤ 0.15 $p \leq 0.030$ S ≤ 0.035
ZQD-SP-104171	62 × 202 × 0.51	0.5–1.15	
QD24	51 × 102 × 0.51	≤0.5	

2.11. Study of Physico-Mechanical Properties

The mechanical properties of the non-pigmented polyacrylate films were studied using standardized tests. The relative surface hardness of the coating films deposited on the glass panels was measured according to ISO 1522 [55] using a Persoz pendulum apparatus (Persoz NF T 30-016, Braive Instruments; Liège, Belgium). The gloss of the coating films applied on the glass panels was determined with a micro-TRI-gloss (µ) (BYK-Gardner; Geretsried, Germany) using the geometry for gloss measurement at 60° according to ISO 2813 [56]. In addition, the resistance of the coating films to impact with a weight (1000 g) from the maximum height at which the coating film remained intact, according to ISO 6272-2 [57], was evaluated using an Elcometer 1615 (Elcometer; Manchester, UK) [58]. The resistance of the films to cracking or peeling was also studied using the cupping test according to ISO 1520 [59]. The latex films were subjected to step deformation by pushing a 20 mm-in-diameter steel ball using an Elcometer 1620. The flexural resistance of the latex films was evaluated through a cylindrical mandrel according to ISO 1519 [60] using an Elcometer 1506. The evaluation of the degree of adhesion of the coatings on steel panels was carried out according to ISO 2409 [61] using a special Elcometer K1542 Cross-Cut Tester cutting knife with a blade spacing of 2 mm. The cross-section of the grid pattern was subjectively rated on a scale from 0 to 5, where 0 indicated the best adhesion [62].

2.12. Determination of Chemical Resistance

The chemical resistance of the non-pigmented films to water exposure was determined depending on the pH level of the corrosion environment. The chemical resistance of the coatings was evaluated on steel panels with a coating layer on which glass rollers were glued. An aqueous buffer solution of different pH levels (2, 4, 6, 8, 10, and 12) was poured into each glass roller. The buffers were prepared from 0.04 M H_3BO_3, 0.04 M H_3PO_4, 0.04 M CH_3COOH, and 0.2 M NaOH solutions. The solutions were left in the rollers for three days, and then the coating surface was evaluated according to ASTM D 610-08 [63] and ASTM D 714-02 [64].

2.13. Corrosion Resistance

The determination of the corrosion resistance of polyacrylate latex paint films was carried out using a cyclic corrosion test in an environment of 5% NaCl mist (modified according to ISO 9227 [65]) in a test chamber (SKB 400 A-TR-TOUCH, Gebr. Liebisch GmbH & Co. KG; Bielefeld, Germany). Testing of individual polyacrylate coating films in both acidic and alkaline form was carried out in 12 h cycles divided into three parts: 10 h of exposure to a mist of a 5% solution of NaCl at a temperature of 38 °C; 1 h of exposure at a temperature of 23 °C; and 1 h of moisture condensation at a temperature of 40 °C. The total exposure time was 120 h. Test samples treated with sealing self-adhesive tape were provided with an 8 cm-long test cut. After exposure, the corrosion manifestations were evaluated according to the relevant standards, such as standard ASTM D714-02's testing method for evaluation of the degree of blistering and ASTM D 610-85's method for evaluation of the degree of corrosion on steel substrate, and assessment of the degree of delamination was carried out following ISO 4628-8 [66].

For each coating film, the spontaneous corrosion potential (E_{corr}), the slopes of the Tafel guidelines (β_a and β_c), the current density (I_{cor}), the polarization resistance (R_p), and the corrosion rate (v_{cor}) were determined using the electrochemical linear polarization technique [67]. The determinations were carried out in electrochemical cells consisting of a working electrode formed by the test sample, a reference saturated calomel electrode, and a platinum counter electrode. Test specimens of the defined areas were exposed to a 3.5 M solution of NaCl electrolyte for 24 h, during which time the spontaneous corrosion potential was measured. After 24 h of exposure, the polarization curves were recorded using the electrochemical linear polarization technique, followed by an evaluation of the linear stretch of these polarization curves in the vicinity of the corrosion potential. Determining the polarization resistance assumes that the central part of the resulting polarization curve of the corrosion system is linear near the corrosion potential and intersects the zero current density axis at a certain angle. The polarization resistance corresponds to the inverse of the linear extrapolation line directive.

3. Results and Discussion

3.1. Chemical Structure of Polypyrrole

The molecular structure of the polypyrrole component synthesized during emulsion polymerization of acrylates was studied using FTIR spectroscopy. The infrared spectrum of polypyrrole prepared with the "one-pot" synthesis strategy (Figure 1) was compared with the spectra of polypyrrole salt (Figure 1, conducting form), the polypyrrole base (deprotonated form) [68], and the spectrum of the Disponil FES 993 emulsifier (Figure 2). In the spectrum of polypyrrole salt, we observed bands with local maxima at 1537 cm^{-1} (C–C stretching vibrations in the pyrrole ring), 1450 cm^{-1} (C−N stretching vibration in pyrrole ring), a broad band at about 1303 cm^{-1} (in-plane deformation vibrations of C–H or C–N bonds), and 1164 cm^{-1} (the band associated with the deformation vibrations of pyrrole rings) [68]. The spectrum also included a peak situated at 1089 cm^{-1} associated with $N-H^+$ deformation vibrations, a sharp peak situated at 1035 cm^{-1} (C–H and N–H in-plane deformation vibrations), and a peak at 904 cm^{-1} (C–H deformation vibration of pyrrole ring) (Figure 2). In the spectrum of polypyrrole synthesized in the present study, we detected bands with maxima at 1537, 1089, 1305, and 904 cm^{-1}, which corresponded to the vibrations of the polypyrrole base. We can thus conclude that the polypyrrole in the present study was partly deprotonated. This was the result of the lower acidity of the reaction medium due to the use of an ammonium peroxodisulfate oxidizing agent instead of the strongly acidic ferric chloride currently used in the literature [68]. The bands at 2925 and 2850 cm^{-1} (C–H stretching vibrations) and a double band with maxima at 1243 and 1209 cm^{-1} reflect the presence of Disponil emulsifier adsorbed at the polypyrrole surface. The bands with maxima at 3428 and 1635 cm^{-1} belong to the vibrations of water molecules.

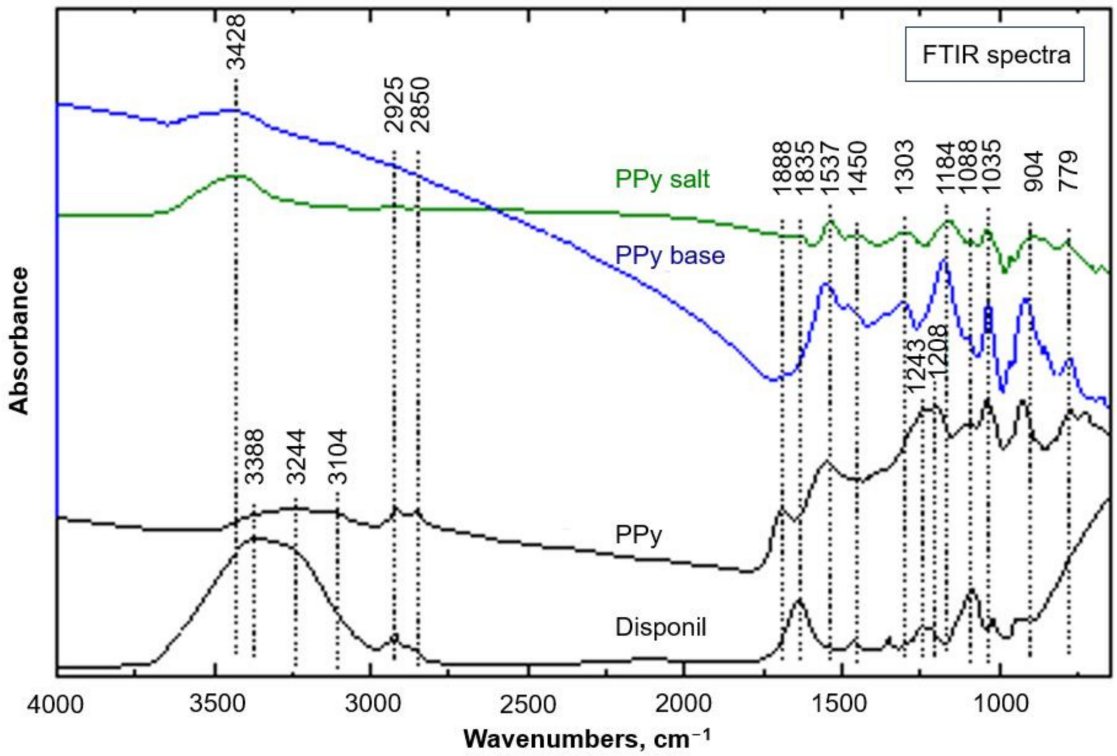

Figure 1. FTIR spectrum of polypyrrole (PPy) prepared with "one-pot" synthesis in the absence of polyacrylate latex polymer compared with the spectra of the polypyrrole salt and base reported in the literature [68].

In the Raman spectrum of the reference conducting polypyrrole salt (Figure 2), we observed a band with a maximum situated at 1590 cm^{-1} (stretching of C=C bonds and inter-ring C–C mode in the backbone of the polaron structure), which shifted to a higher frequency after deprotonation to the polypyrrole base [68]. We also detected two maxima at 1387 and 1323 cm^{-1} (inter-ring stretching vibrations of C–C bonds of polypyrrole), where the peak appearing at a higher frequency was assigned to the asymmetric inter-ring stretching C–N vibrations in conducting polypyrrole salt while the lower-frequency side peak was assigned to the deprotonated polypyrrole base. This band increased after deprotonation. The band with a maximum at 1254 cm^{-1} was associated with asymmetric C–H in-plane bending vibrations. In the double band observed at 1082 and 1048 cm^{-1}, the maximum at the higher frequency was assigned to the in-plane deformation vibrations of the C–H bonds. The intensity of this band decreased after deprotonation. The maximum at a lower frequency of 1048 cm^{-1} corresponded to non-protonated polypyrrole units, and its intensity increased after deprotonation. The bands with maxima situated at 984 and 933 cm^{-1} were assigned to the ring in-plane deformation and associated with the polaron and bipolaron states of polypyrrole, respectively. The band attributed to the ring deformation of the non-protonated polypyrrole segment appeared at 922 cm^{-1}. The C–H out-of-plane deformation band was observed at 688 cm^{-1}. The spectrum of the polypyrrole prepared with the "one-pot" synthesis strategy in the absence of acrylic monomers was close to the spectrum of the polypyrrole base (Figure 2). We can conclude that the polypyrrole component formed during emulsion polymerization was polypyrrole which was protonated only in part, also in accordance with the FTIR spectra.

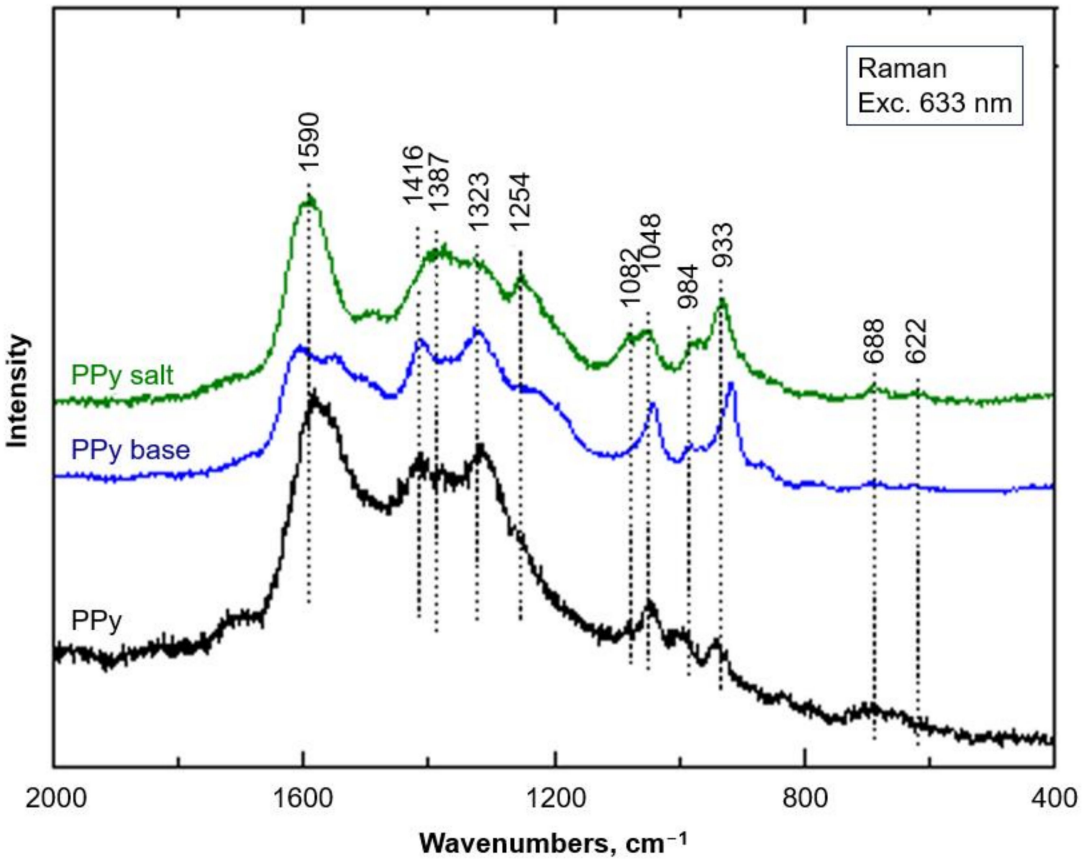

Figure 2. Raman spectrum of polypyrrole (PPy) prepared with "one-pot" synthesis in the absence of polyacrylate latex polymer compared with the spectra of the polypyrrole salt and base reported in the literature [68].

3.2. Basic Properties of Latices

Polypyrrole is typically prepared through the chemical oxidation of pyrrole with ferric chloride [69] or ammonium peroxodisulfate [70] (Figure 3). The latter oxidizing agent was selected for this study to avoid the presence of chloride anions in the formulations. Sulfuric acid is a byproduct, and the acidity of the medium thus increases during polymerization. Polypyrrole is obtained as a conducting salt with sulfate counter-ions.

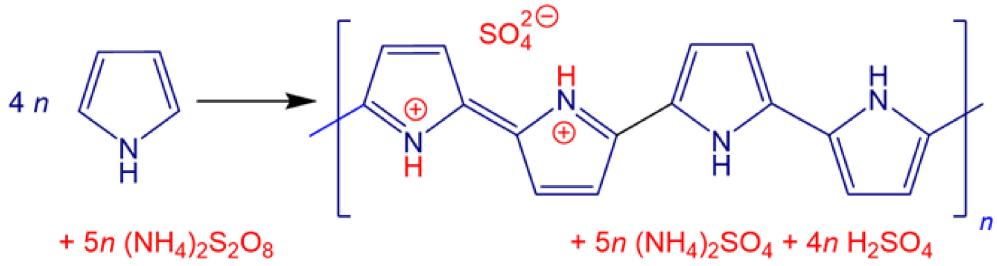

Figure 3. Oxidation of pyrrole in aqueous medium yields polypyrrole salt.

The characteristic properties of the heterogeneous latices comprising both polyacrylate and polypyrrole components are summarized in Table 3. The latices L_{acid_0} and $L_{acid\_0.25}$ were close regarding solids and coagulum content. On the contrary, an increase in the coagulum content and decrease in solids was found in the case of the latex sample $L_{acid\_0.50}$ synthesized with the highest pyrrole dosage, indicating a decrease in colloidal stability during the "one-pot" synthesis. This latex sample also exhibited a pronouncedly decreased value of monomer conversion, probably due to considerable consumption of ammonium

peroxodisulfate during the oxidative polymerization of pyrrole. Therefore, the initiation of the radical polymerization of acrylate monomers at a pyrrole dosage of 0.5 wt. % was not sufficiently efficient, and low values of conversion and solids were found. The pH levels of individual latices gradually decreased from 1.9 to 1.6. The drop in pH was caused by the decomposition of ammonium peroxodisulfate in water [71,72] and its reaction with pyrrole to form sulfuric acid as a byproduct (Figure 3). The increasing amount of ammonium peroxodisulfate also led to an increase in the ionic strength of the dispersion medium. These phenomena and the probable precipitation and accumulation of polypyrrole on the polyacrylate latex particle surface (resulting in the surface's negative charge decreasing due to the polypyrrole overlayer coating) could result in flocculation of latex particles and the mentioned increase in coagulum content.

Table 3. Basic characteristics of prepared latices.

Latex	Coagulum (wt. %)	Conversion (%)	Solids (wt. %)	pH	T_g (°C)	MFFT (Acidic Latex) (°C)	MFFT (Alkaline Latex) (°C)
L_{acid_0}	0.4	99.8	39.0	1.9 ± 0.1	0.4 ± 0.2	8.1 ± 0.1	7.7 ± 0.2
$L_{acid\_0.25}$	0.5	97.9	38.8	1.7 ± 0.1	3.4 ± 0.4	10.0 ± 0.3	8.0 ± 0.2
$L_{acid\_0.50}$	1.9	66.3	29.4	1.6 ± 0.1	4.5 ± 0.5	11.5 ± 0.2	8.3 ± 0.3

DSC analysis of the prepared heterogeneous latex materials revealed only one detectable glass transition corresponding to the polyacrylate matrix. The glass transition corresponding to the polypyrrole component was not detected, in all probability, due to the low content of the polypyrrole phase. However, the T_g of polypyrrole synthesized by blank "one-pot" emulsion polymerization (following the procedure for the latex sample with a pyrrole dosage of 0.5 wt. %, except that no acrylate monomers were introduced into the polymerization system) was determined to be approximately 84 °C. Nevertheless, with the increasing polypyrrole loading, a slight increase in T_g was noted, which was probably caused by the presence of polypyrrole in the polyacrylate matrix. The MFFT of the latices in acidic form ranged from 8.1 to 11.5 °C. Thus, all of the polyacrylate latices were already able to form a coating film at room temperature. Alkalization of the latices resulted in a reduction in the MFFT, which decreased with increasing polypyrrole loading. The decrease in the MFFT of the alkaline latices can be explained by the observed decrease in radical polymerization conversion, which resulted in a decrease in the molecular weight of the polyacrylate latex polymer. Alternatively, the deprotonation of polypyrrole salt (Figure 1) to a base [68] could also be responsible for the observed effects.

3.3. Stability of Latices

The particle diameter and zeta potential of latices were determined for both the acidic and alkaline latices (Table 4). The latex samples synthesized with 0 and 0.25 wt. % pyrrole dosages showed similar particle diameters and low polydispersity values, with the latter data indicating monomodal and narrow particle size distributions. On the contrary, significantly increased particle diameters and polydispersity values were found for the latex samples synthesized with a 0.5 wt. % pyrrole dosage. This fact is indicative of decreased stability and the flocculation of latex particles. Moreover, these samples also showed a bimodal particle size distribution, where the presence of the polypyrrole component could be assumed in the higher particle size fraction. The information regarding colloidal stability is further associated with the zeta potential [73], showing sufficiently high absolute values (i.e., stability in the case of latices synthesized with 0 and 0.25 wt. % pyrrole dosages), while the latices synthesized with a 0.5 wt. % pyrrole dosage exhibited decreased absolute values for the zeta potential, indicating reduced latex stability. This phenomenon may indicate the precipitation of polypyrrole on the polyacrylate latex particle surface, forming composite particles with polypyrrole overlayer coatings. Thus, the polyacrylate latex particles lost

their carboxyl and sulfate group-based surface negative charge and flocculated due to the lack of charge.

Table 4. Results from DLS and storage stability testing at 40 °C (1 and 4 months) and 60 °C (24, 48, and 120 h) [a].

Latex	Zeta Potential (mV)	Particle Diameter (nm)		Polydispersity (%)	1 Month	4 Months	24 h	48 h	120 h
		Peak 1	Peak 2						
L_{acid_0}	−37.4 ± 0.7	137 ± 1	-	2.6 ± 1.7	0	0	0	0	X
$L_{acid\_0.25}$	−38.4 ± 1.3	130 ± 2	-	3.3 ± 2.1	0	0	0	0	X
$L_{acid\_0.50}$	−30.2 ± 1.5	253 ± 27	1074 ± 373	28.0 ± 2.0	0	0	0	0	X
L_{alkali_0}	−38.4 ± 0.8	147 ± 1	-	3.8 ± 2.7	0	0	0	0	0
$L_{alkali\_0.25}$	−40.1 ± 1.9	138 ± 2	-	2.5 ± 1.4	0	0	0	0	X
$L_{alkali\_0.50}$	−33.1 ± 1.0	313 ± 33	1112 ± 447	28.3 ± 3.3	0	0	0	0	X

[a] Stability results expressed with the symbol "0" mean that no visible coagulation occurred, and the latex provided coatings with preserved gloss. "X" means that visible coagulation occurred.

From the point of view of application in paints, the binders must have satisfactory stability under various environmental conditions [74]. For this reason, the latices were evaluated for their stability during storage for 4 months at 40 °C (Table 4). All latices remained stable during storage at this temperature. The stability of the latices was also evaluated at 60 °C for 24, 48, and 120 h. All latices remained stable at 60 °C for 48 h. Except for the latex L_{alkali_0}, the coagulum formation was observed in the case of all latices after 120 h exposure. The enhanced thermal stability of the latex L_{alkali_0} can be related to the increased surface charge of polyacrylate particles due to alkalization [75] and the absence of a polypyrrole overlayer coating.

3.4. Presence of Polypyrrole Component in Latex Film

The morphology and distribution of the polypyrrole component in the coating films were studied using SEM and AFM. The pyrrole monomer was assumed to polymerize in an aqueous solution or on the polyacrylate particle surface. (Pyrrole polymerization within the polyacrylate particle interior was highly unlikely because the water-soluble ammonium peroxodisulfate oxidant should not diffuse into the hydrophobic polyacrylate particles). The polypyrrole component was expected to be precipitated solely in the aqueous medium or accumulated on the polyacrylate particle surface to minimize the interfacial free energy [76]. Considering the fact of a zeta potential decrease being observed in the case of $L_{acid\_0.50}$ and $L_{alkali\_0.50}$ (suggesting the loss of the surface negative charge on latex particles due to the polypyrrole overlayer), the formation of composite polypyrrole-coated polyacrylate latex particles is the most probable idea, which is also consistent with the findings in the literature [26,34,35].

Cryo-fracture micrographs of free-standing coating films prepared from alkaline latices examined via SEM revealed irregular (elongated) submicron particles in the cases of the $L_{alkali\_0.25}$ and $L_{alkali\_0.50}$ coatings (Figure 4b,c). The size of these particles, probably having the nature of isolated or aggregated composite polyacrylate particles with polypyrrole overlayer coatings, slightly increased with the level of polypyrrole loading. The real content of the polypyrrole component in dry-coating films was estimated according to the elemental analysis results (Table 5). The nitrogen concentration was used to assess the content of polypyrrole. Although the presented results represent only a rough approximation, it can be stated that the real concentration of the polypyrrole component in the latex coatings increased with an increasing pyrrole dosage. Note that the non-negligible nitrogen concentration in the reference sample is attributed to the ammonium peroxodisulfate initiator and the presence of the alkalizing agent.

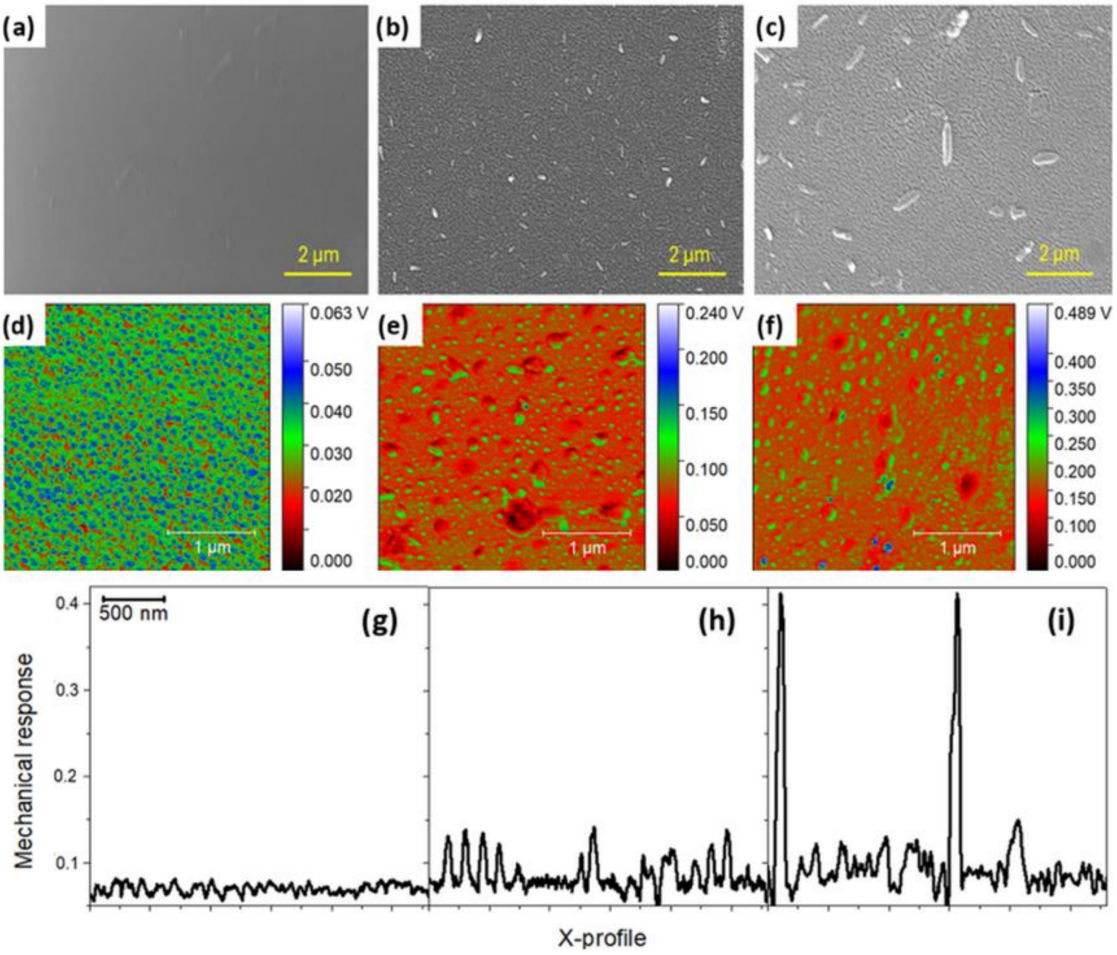

Figure 4. Fracture surface topography of the coating films obtained via SEM: (**a**) L_{alkali_0}, (**b**) $L_{alkali\_0.25}$, and (**c**) $L_{alkali\_0.50}$. Mechanical maps (below) determined via AFM for the coating films (**d**) L_{alkali_0}, (**e**) $L_{alkali\_0.25}$, and (**f**) $L_{alkali\_0.50}$. (**g–i**) Corresponding profiles of mechanical response.

Table 5. Results for nitrogen concentration and polypyrrole content obtained using elemental analysis.

Latex	N Concentration (wt. %)		Polypyrrole Content (wt. %)	
	Total—Experimentally Determined	Calculated for Polypyrrole [a]	Theoretical	Experimentally Determined [a]
L_{alkali_0}	0.18 ± 0.01	0	0	0
$L_{alkali\_0.25}$	0.31 ± 0.01	0.037	0.24	0.18
$L_{alkali\_0.50}$	0.49 ± 0.07	0.091	0.48	0.44

[a] Calculations were based on the difference in the experimentally determined N concentrations between the polypyrrole-containing sample and the reference sample (L_{alkali_0}) using the starting amounts of the individual reaction components under the simplifying assumption that the remaining content of the alkalizing agent was the same in all latex samples.

When using AFM in mechanical mode, some grainy features describing the relics of the original latex polymer spheres were observed in the coating film prepared from $L_{\_alkali\_0}$ latex (see Figure 4d,g) The lateral size of these relicts was 110–120 nm, which corresponds well with the size of the original primary latex particles according to DLS (137 nm; Table 4). The slight reduction in size was due to the combined effects of coalescence, particle drying, and detection of the double layer by the DLS technique. The total contrast of the mechanical response (the slope of the force spectroscopy; see [77,78]) was quite homogeneous and connected with some topographical differences. In the cases of the coatings prepared from $L_{alkali\_0.25}$ and $L_{alkali\_0.50}$, two types of new particles with significantly higher stiffness values appeared in the mechanical response. In the case of the coating film from $L_{alkali\_0.25}$,

the given particles were marked in green (Figure 4e). The full-width-at-half-maxima (FWHM) was in the range of 40–80 nm, and the change in mechanical response was three times higher than the response of the reference latex $L_{\_alkali\_0.2}$ (Figure 4h). For the coating from $L_{alkali\_0.5}$, there was a more pronounced separation of several particles with a mechanical response close to 0.5 V (see blue areas). (For comparison, the mechanical response of the $L_{\_alkali\_0}$ coating was below 0.07 V.) Due to the change in mechanical properties with the addition of the polypyrrole component, it can be concluded that the polypyrrole was not fully dispersed (in a supramolecular manner) in the material but was localized in nanoscale grains in which the polypyrrole concentration increased with the concentration in the sample, consistent with Cahn–Hilliard effects [79].

3.5. Characterization of the Pigments

For this work, inorganic pigments from the group of oxides and sulfides of transition metals (ZnO, ZnS, and MoS_2), zinc ferrite (mixed oxide) prepared via high-temperature synthesis in the solid phase and an industrially used pigment $Zn_3(PO_4)_2$ were selected, for which their basic characterization was carried out. Typical parameters such as the oil number and density, which are necessary to calculate the critical pigment volume concentration (CPVC), were determined. Furthermore, photomicrographs of the individual pigments were taken, and the particle size was determined from the photomicrographs (Figure 5) taken using a scanning electron microscope (SEM). The results of the studied pigments are summarized in Table 6. The densities of individual pigments ranged from 3.35 g·cm^{-3} ($Zn_3(PO_4)_2$) to 5.68 g·cm^{-3} (ZnO). Individual pigments achieved oil absorption values ranging from 21.5 to 29.8 g/100 g. The oil absorption parameter is closely related to the porosity of the pigment particles as well as their surface and shape. The lowest oil absorption values were determined for the ZnO pigment (15.3 g/100 g), which showed small particles of an isometric shape with a particle size distribution of 100–300 nm, and the ZnS pigment (15.8 g/100 g), which according to SEM scans formed polycrystalline spherical clusters with a tetrahedral shape for the primary particles (100–200 nm). On the contrary, higher values of oil absorption were found for the pigments $Zn_3(PO_4)_2$ and MoS_2 (33.9 and 29.8 g/100 g). The MoS_2 particles showed a typical layered structure, while the $Zn_3(PO_4)_2$ particles were polycrystalline clusters with a non-isometric shape. CPVC values ranged from 39.4 (MoS_2) to 59.3 (ZnS).

3.6. Physico-Mechanical Properties

Since latex coating binders are usually used in a neutralized state [80], only the coating films made from alkaline latices were subjected to physico-mechanical testing. The physical properties and mechanical resistance of the non-pigmented coatings (DFT of 60 ± 5 µm) are shown in Table 7. All coating samples displayed a highly glossy, smooth, and slick surface without any bubbles or defects. The high gloss indicates the presence of nano-sized particles and good coalescence of these coating films. On the contrary, the coating from the latex $L_{alkali\_0.5}$ exhibited a significant decrease in gloss, which can be attributed to a higher content of ionic species (originating especially from the increased dosage of ammonium peroxodisulfate) which were excluded on the coating surface during film formation. The Persoz surface hardness measurements showed that the hardness of the coating films increased with increased polypyrrole loading (Table 7), probably due to the improved effect of ionic interfacial crosslinking between polypyrrole polycation and the carboxyl groups in the binder. Further mechanical property tests showed that coatings from the latex $L_{alkali\_0.50}$ exhibited lower impact toughness, which can be attributed to a decrease in the molecular weight of the polyacrylate latex polymer [81], as suggested earlier. Nevertheless, all films provided the maximum possible rating in the cupping and bending tests and exhibited high adhesion to the steel substrate, rated at grade zero. Therefore, it can be concluded that the polypyrrole component did not significantly affect the otherwise excellent mechanical properties.

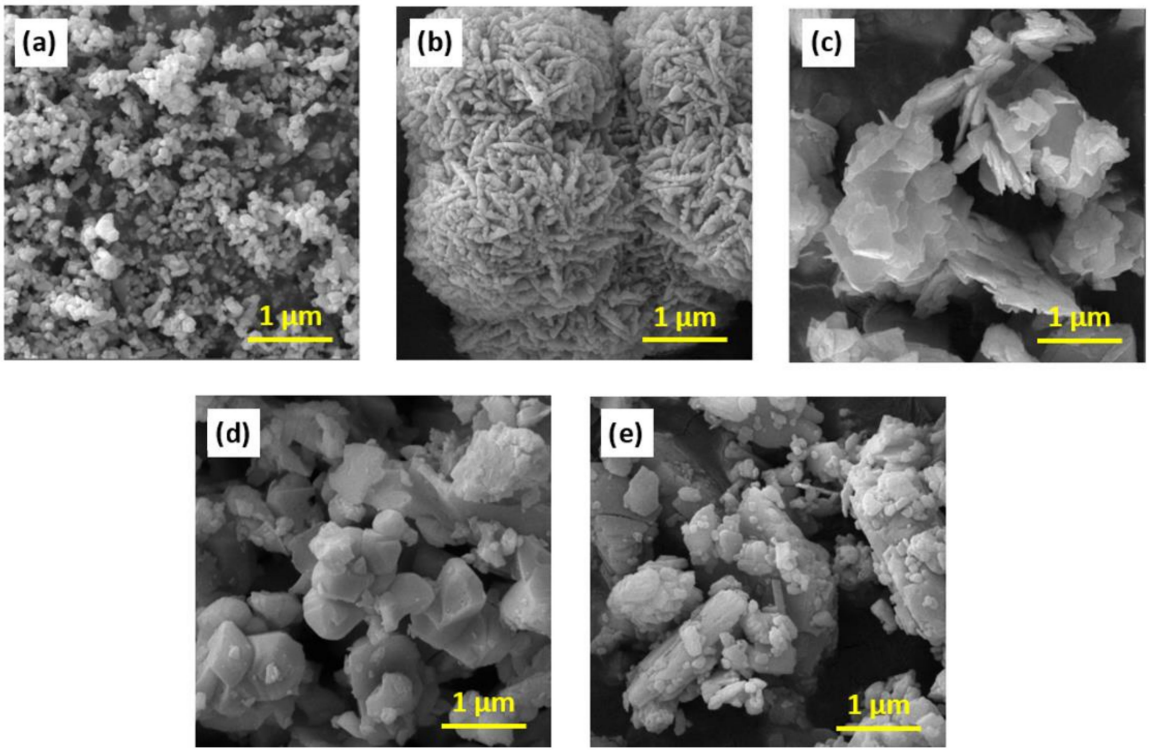

Figure 5. SEM micrographs of the inorganic pigments used: (**a**) ZnO, (**b**) ZnS, (**c**) MoS_2, (**d**) $ZnFe_2O_4$, and (**e**) $Zn_3(PO_4)_2$.

Table 6. Basic physicochemical properties of used pigments.

Pigment	Oil Absorption (g/100 g)	Density ($g \cdot cm^{-3}$)	CPVC	Size of Primary Particles (µm)
ZnO	15.3 ± 0.2	5.68 ± 0.02	51.7	0.2 ± 0.1
ZnS	15.8 ± 0.2	4.04 ± 0.02	59.3	0.3 ± 0.1
MoS_2	29.8 ± 0.2	4.81 ± 0.02	39.4	1.3 ± 0.6
$ZnFe_2O_4$	24.1 ± 0.2	5.17 ± 0.02	42.7	1.2 ± 0.6
$Zn_3(PO_4)_2$	33.9 ± 0.2	3.35 ± 0.02	45.0	1.1 ± 0.7

Table 7. Physico-mechanical properties of alkali-treated non-pigmented coatings.

Latex	Gloss (60°)	Hardness (%)	Impact (cm)	Cupping (mm)	Bending (mm)	Adhesion (dg.)
L_{alkali_0}	147.1 ± 0.5	38.6 ± 0.1	60	>10	<2	0
$L_{alkali\_0.25}$	130.6 ± 0.1	39.6 ± 0.1	60	>10	<2	0
$L_{alkali\_0.50}$	110.0 ± 0.3	40.5 ± 0.1	50	>10	<2	0

3.7. Chemical Resistance

The chemical resistance of the non-pigmented coatings (DFT of 60 ± 10 µm) cast on steel panels was evaluated after exposure for 72 h to buffer solutions of pH = 2, 4, 6, 8, 10, and 12 (Table 8). The results show that the coatings made from the latices in alkaline form were more chemically resistant than those originating from the latices in acidic form. The highest chemical resistance was achieved by the coating film from the latex $L_{alkali\_0.25}$, which showed no change in the appearance after 72 h of exposure to buffers at pH = 2–8, with only isolated blistering at pH = 10 and wrinkling of the coating film at pH = 12. Similar values were achieved by the coating film originating from the latex L_{alkali_0}. On the other hand, the films from the latices synthesized at higher polypyrrole loadings ($L_{acid\_0.50}$ and $L_{alkali\_0.50}$) contained a large amount of blistering at most pH values, and at pH = 10–12, the coating

films wrinkled and even lost their integrity. After finishing the chemical resistance testing, the coating films were removed using a paint stripper (Green Paint Stripper; manufacturer: Rust Oleum), and the corrosion degree of the steel substrate was evaluated (Table 8). The results of the degree of corrosion and the chemical resistance determination corresponded with each other. The steel panel with a coating originating from the latex $L_{alkali\_0.25}$ had the lowest degree of corrosion, with corrosion ranging from 1 to 3% at all pH values.

Table 8. Chemical resistance of non-pigmented coatings and degree of corrosion of coated steel substrate induced by aqueous buffers of different pH levels.

Latex	Changes in the Coating Quality [a]						Corrosion of Coated Steel (%)					
	2	**4**	**6**	**8**	**10**	**12**	**2**	**4**	**6**	**8**	**10**	**12**
L_{acid_0}	0	0	0	0	2	2	16	3	16	10	33	33
$L_{acid\_0.25}$	2	1	1	1	3	3	33	10	16	10	33	33
$L_{acid\_0.50}$	2	2	2	3	4	4	10	10	10	10	3	3
L_{alkali_0}	0	0	0	0	2	3	16	16	10	3	10	50
$L_{alkali\_0.25}$	0	0	0	0	1	3	3	1	1	3	1	1
$L_{alkali\_0.50}$	2	2	2	0	3	3	50	33	33	16	3	3

[a] 0 = no change; 1 = isolated blistering; 2 = blistering over the entire area; 3 = wrinkling (loss of adhesion); 4 = upsetting the integrity of the film.

3.8. The Corrosion Protective Efficiency of Non-Pigmented Coatings

3.8.1. Cyclic Corrosion Test in a 5% Salt Spray Atmosphere

Polyacrylate coating films applied to steel panels were subjected to a cyclic corrosion test in a neutral salt fog environment for 120 h, where corrosion manifestations were subsequently evaluated. The results are shown in Table 9. Photographs of individual coating films after 120 h of exposure are shown in Figure 6. The anticorrosion efficiency of the non-pigmented polyacrylate latex films in acidic form was lower compared with the latex coating films in alkaline form. However, a positive effect of the presence of the polypyrrole component was observed here; as with the coating film made from the reference latex without the content of polypyrrole, blisters occurred in the surface of the coating film and around the test section, rated as 8F after 48 h of exposure, while in the case of coating films from latices $L_{\_acid\_0.25}$ and $L_{\_acid\_0.5}$, even after 120 h, no blisters appeared on the surface or in the test section. In addition, the coating film made from latex $L_{\_acid\_0}$ showed higher corrosion around the test cut in the range of 3–3.5 mm, and the corrosion in the coating area and corrosion of the steel substrate was near 1%. The highest anti-corrosion efficiency was achieved by the coating film made of latex $L_{\_acid\_0.25}$, where there were no blisters either on the surface of the coating film or in the test section. In addition, this system also showed rather little corrosion on the surface of the paint film and the steel substrate, being approximately 0.3%. The paint films made of polyacrylate latices in alkaline form showed higher anti-corrosion efficiency compared with the paint films in acid form. They have been shown to have less corrosion in the section and a lower tendency for corrosion on the surface of the paint film. However, with the coating film made from the reference latex $L_{\_alkali\_0}$, blisters rated at 8M already appeared in the vicinity of the test cut after 72 h. The highest anti-corrosion efficiency was achieved by the coating film made of latex $L_{\_alkali\_0.25}$, which did not have any blisters either in the area or in the test cut. In addition, the corrosion in the surface of the coating film was a minimum of 0.03%. Comparable results were also achieved by the $L_{\_alkali\_0.5}$ latex paint film, which also did not have any blisters in the test cut or on the surface of the paint film, and the corrosion on the surface of the paint film was only 0.3%.

Table 9. Anti-corrosion resistance of non-pigmented coatings after 120 h exposure in a 5% salt spray atmosphere. DFT = 90 ± 10 µm.

Latex	Blistering		Corrosion		
	In the Cut (dg.)	On the Film Area (dg.)	In the Cut (mm)	On the Film Area (%)	Metal Base (%)
L_{acid_0}	8F	8F	3–3.5	1	1
$L_{acid\_0.25}$	-	-	1–1.5	0.3	0.3
$L_{acid\_0.50}$	8M	-	1–1.5	10	10
L_{alkali_0}	8M		1–1.5	3	3
$L_{alkali\_0.25}$	-	-	0.5–1	0.03	0.03
$L_{alkali\_0.50}$	-	-	0.5–1	0.3	0.3

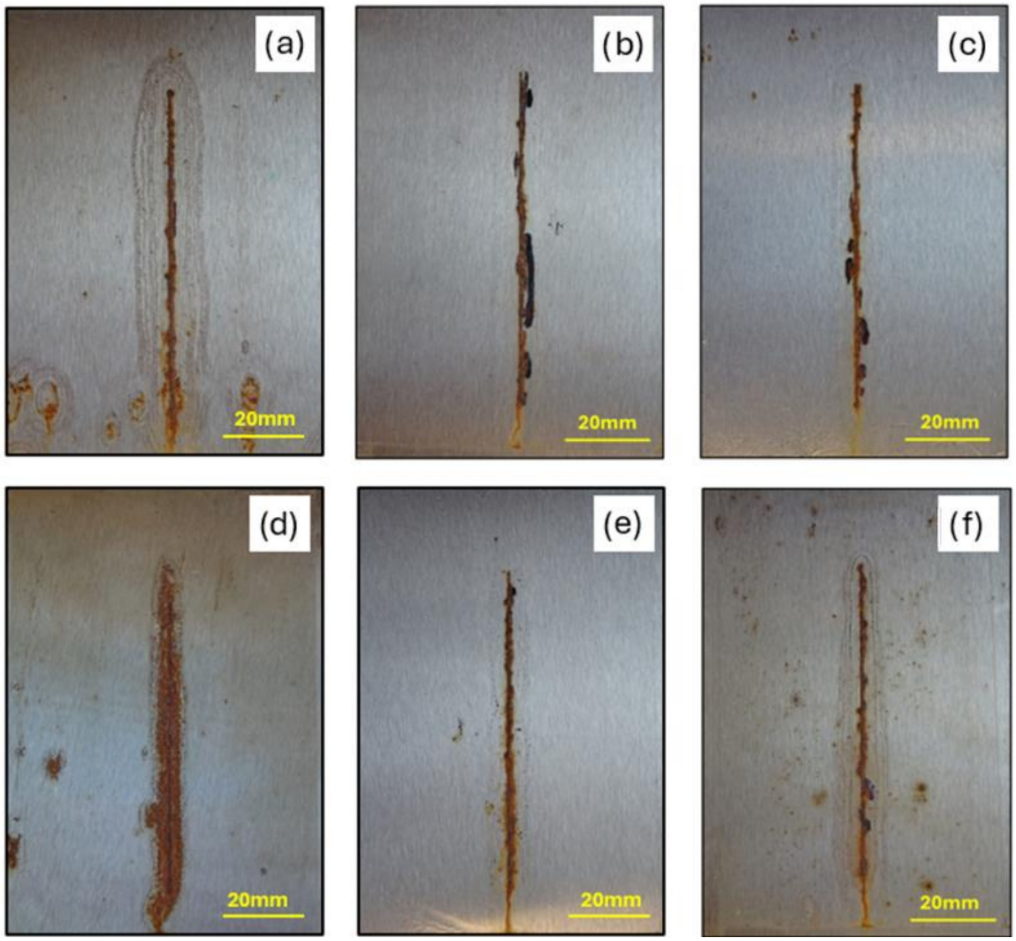

Figure 6. Non-pigmented coatings on steel substrates after 120 h of exposure in a 5% salt spray atmosphere: (**a**) L_{alkali_0}, (**b**) $L_{alkali\_0.25}$, (**c**) $L_{alkali\_0.50}$, (**d**) $L_{acid\_\_0}$, (**e**) $L_{acid\_0.25}$, and (**f**) $L_{acid\_0.50}$.

3.8.2. Electrochemical Technique of Linear Polarization

The corrosion resistance of the non-pigmented polyacrylate latex films with DFT = 60 ± 10 µm was evaluated with the electrochemical technique of linear polarization. Using this technique, individual polarization curves were measured after the spontaneous corrosion potential had stabilized. First, the cathodic parts of the curve were measured followed by the anodic parts of the curve, because when measuring the anodic part of the curve, there were changes in the measured surface of the sample. The sum curve was experimentally verified by this procedure, which was curved in semilogarithmic coordinates in the vicinity of the corrosion potential and had a linear course at higher potentials. The linear region on the curve was called the tafel region, by extrapolation of

which it was possible to determine the corrosion current density I_{corr} (i.e., an indicator of the corrosion rate), the corrosion potential E_{corr}, and last but not least the slopes of the tafel regions $ß_a$ and $ß_c$. The polarization resistance R_p was evaluated from a linear section near the corrosion potential, where the inverse of the directive value of this linear section gives the polarization resistance. Based on the above parameters, the corrosion rate v_{corr} was also calculated for each coating film [82–86].

The parameters determined by the electrochemical technique of linear polarization for the non-pigmented polyacrylate latex films are shown in Table 10. The spontaneous corrosion potential of the coating films cast from all types of acid latices ranged from −623 to −534 mV, where the lowest value of the current density was recorded for the coating film from the latex $L_{acid\_0.25}$. The highest polarization resistance value of 0.88 MΩ and the lowest corrosion rate value of 1.33×10^{-4} mm/year were also recorded for this film. The study of the alkalized latices and their corresponding coating films, where the spontaneous corrosion potential ranged from −491 to −474 mV, clearly show that there was an increase in corrosion resistance when compared with the acid latices, as evidenced by the increase in the polarization resistance values of the individual samples. The highest value of polarization resistance was determined for the latex coating $L_{alkali\_0.25}$, which reached a value of 0.99 MΩ, while the lowest value of corrosion rate was 1.12×10^{-4} mm/year.

Table 10. Protective efficiency of non-pigmented coatings determined by the linear polarization technique.

Latex	E_{corr} (mV)	I_{corr} (µA)	$ß_a$ (mV)	$ß_c$ (mV)	R_p (MΩ)	v_{corr} (mm/Year)
L_{acid_0}	–623	1.7×10^{-2}	15.2	17.3	0.19	2.51×10^{-4}
$L_{acid\_0.25}$	–535	9.1×10^{-3}	41.0	35.0	0.88	1.33×10^{-4}
$L_{acid\_0.50}$	–534	2.0×10^{-2}	24.6	23.7	0.26	2.95×10^{-4}
L_{alkali_0}	–474	8.7×10^{-3}	43.1	38.2	0.97	1.13×10^{-4}
$L_{alkali\_0.25}$	–486	8.5×10^{-3}	44.1	39.2	0.99	1.12×10^{-4}
$L_{alkali\_0.50}$	–491	9.1×10^{-3}	34.7	36.9	0.85	1.34×10^{-4}

Based on these measurements, it can be concluded that the coatings cast from the latices $L_{acid\_0.25}$ and $L_{alkali\_0.25}$ achieved higher corrosion resistance values compared with the corresponding types of reference latices without the polypyrrole component. The authors attribute this fact to the demonstrated ability of polypyrrole, where the corrosion potential of the prepared composite coating, due to the presence of an incorporated polypyrrole component in a given type of system, increased the corrosion potential value from –623 mV (L_{acid_0}) to a value of –535 mV ($L_{acid\_0.25}$) [87]. The anti-corrosion efficiency of the given systems with incorporated polypyrrole components also influenced the proven redox properties and conductivity of polypyrrole [88]. Based on these results, the latices without polypyrrole loading and latices prepared at a 0.25 wt. % dose of pyrrole were pigmented with selected types of pigments in the continuation of this study.

3.9. The Corrosion Protective Efficiency of the Pigmented Coatings

The latices synthesized at a 0.25 wt. % pyrrole dosage and the reference latices without polypyrrole in acidic and alkali forms were used for the preparation of pigmented coatings and corrosion resistance testing. The effects of different pigments (ZnO, MoS_2, ZnS, $ZnFe_2O_4$, and $Zn_3(PO_4)_2$) were compared (Tables 11 and 12). SEM micrographs of the film surfaces for the non-pigmented and selected pigmented coatings in alkaline form are shown in Figure 7. Tafel plots of the selected pigmented coatings are shown in Figures 8 and 9. It was found that the presence of the polypyrrole component provided increased corrosion resistance in all pigmented coatings. The pigments exhibited a chemical protective mechanism in the paint films and thus had a beneficial effect on the corrosion protection of latex paint films.

Table 11. Protective efficiency of coatings made from the pigmented original latices L_{acid_0} and $L_{acid\_0.25}$.

Latex/Pigment	E_{corr} (mV)	I_{corr} (μA)	$ß_a$ (mV)	$ß_c$ (mV)	R_p (MΩ)	v_{corr} (mm/Year)
L_{acid-0}/ZnO	−451	1.4×10^{-2}	26.8	27.4	4.2	2.06×10^{-5}
$L_{acid-0.25}/ZnO$	−489	1.3×10^{-2}	26.9	27.3	4.5	1.92×10^{-5}
$L_{acid-0}/Zn_3(PO_4)_2$	−550	3.9×10^{-4}	21.1	19.3	11	5.76×10^{-6}
$L_{acid-0.25}/Zn_3(PO_4)_2$	−552	3.1×10^{-4}	20.7	17.7	13	4.60×10^{-6}
L_{acid-0}/ZnS	−510	3.0×10^{-4}	22.4	20.4	15	4.43×10^{-6}
$L_{acid-0.25}/ZnS$	−508	2.7×10^{-4}	21.2	19.0	14	4.01×10^{-6}
L_{acid-0}/MoS_2	−498	1.2×10^{-5}	21.8	17.4	24	2.80×10^{-6}
$L_{acid-0.25}/MoS_2$	−491	1.2×10^{-4}	21.3	13.7	29	1.83×10^{-6}
$L_{acid-0}/ZnFe_2O_4$	−552	5.9×10^{-3}	27.8	28.7	1.0	8.71×10^{-5}
$L_{acid-0.25}/ZnFe_2O_4$	−581	5.5×10^{-3}	27.2	27.8	1.1	8.12×10^{-5}

Table 12. Protective efficiency of coating films made from the pigmented alkali-treated latices L_{alkali_0} and $L_{alkali\_0.25}$.

Latex/Pigment	E_{corr} (mV)	I_{corr} (μA)	$ß_a$ (mV)	$ß_c$ (mV)	R_p (MΩ)	v_{corr} (mm/Year)
$L_{alkali-0}/ZnO$	−467	1.3×10^{-3}	26.7	27.1	4.6	1.89×10^{-5}
$L_{alkali-0.25}/ZnO$	−410	1.2×10^{-3}	28.3	29.7	5.2	1.77×10^{-5}
$L_{alkali-0}/Zn_3(PO_4)_2$	−598	6.2×10^{-4}	38.8	37.4	13	9.15×10^{-6}
$L_{alkali-0.25}/Zn_3(PO_4)_2$	−514	6.1×10^{-4}	42.4	38.7	14	9.10×10^{-6}
$L_{alkali-0}/ZnS$	−507	5.2×10^{-4}	40.2	37.6	17	7.53×10^{-6}
$L_{alkali-0.25}/ZnS$	−542	3.6×10^{-4}	43.1	45.5	26	5.31×10^{-6}
$L_{alkali-0}/MoS_2$	−608	0.3×10^{-4}	39.8	38.5	28	4.43×10^{-6}
$L_{alkali-0.25}/MoS_2$	−613	2.4×10^{-4}	34.9	33.1	30	3.50×10^{-6}
$L_{alkali-0}/ZnFe_2O_4$	−518	4.7×10^{-3}	26.5	26.9	1.2	6.94×10^{-6}
$L_{alkali-0.25}/ZnFe_2O_4$	−549	4.2×10^{-3}	27.7	28.9	1.5	6.20×10^{-5}

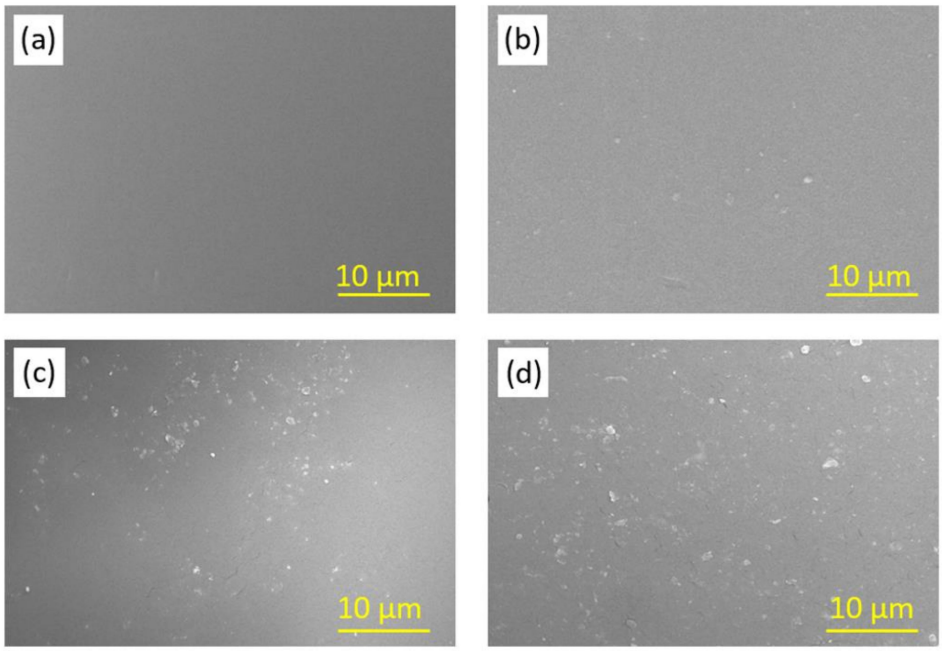

Figure 7. SEM micrographs of coating films prepared from latices: (**a**) L_{alkali_0}, (**b**) $L_{alkali\_0.25}$, (**c**) $L_{alkali\_0.25}/MoS_2$, and (**d**) $L_{alkali\_0.25}/ZnFe_2O_4$.

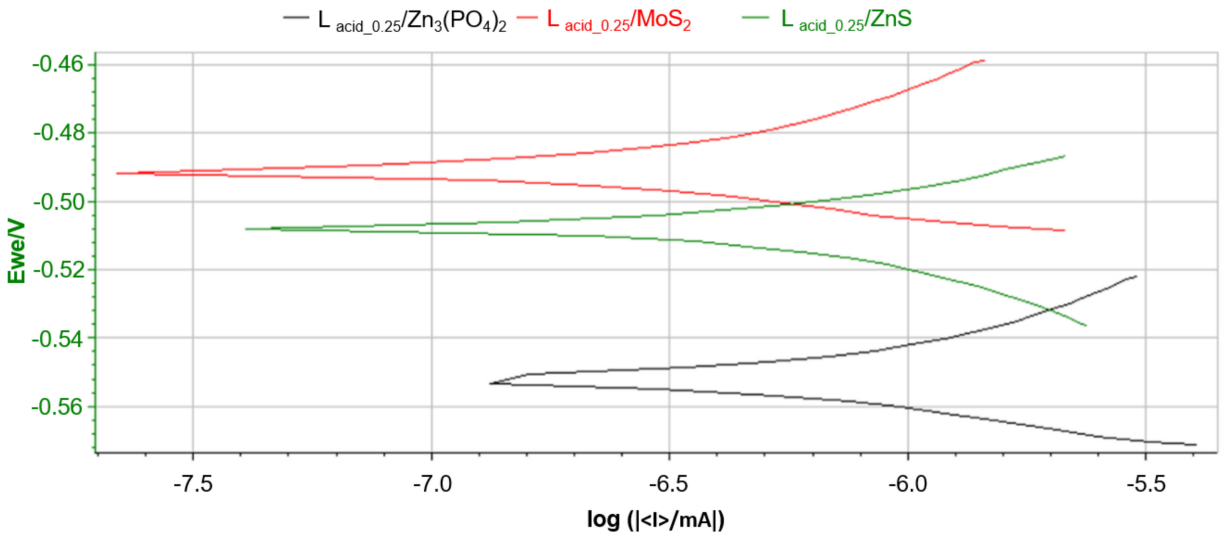

Figure 8. Tafel plots of the selected pigmented coatings: red line for $L_{\_acid\_0.25}/MoS_2$, green line for $L_{\_acid\_0.25}/ZnS$, and black line for $L_{\_acid\_0.25}/Zn_3(PO_4)_2$.

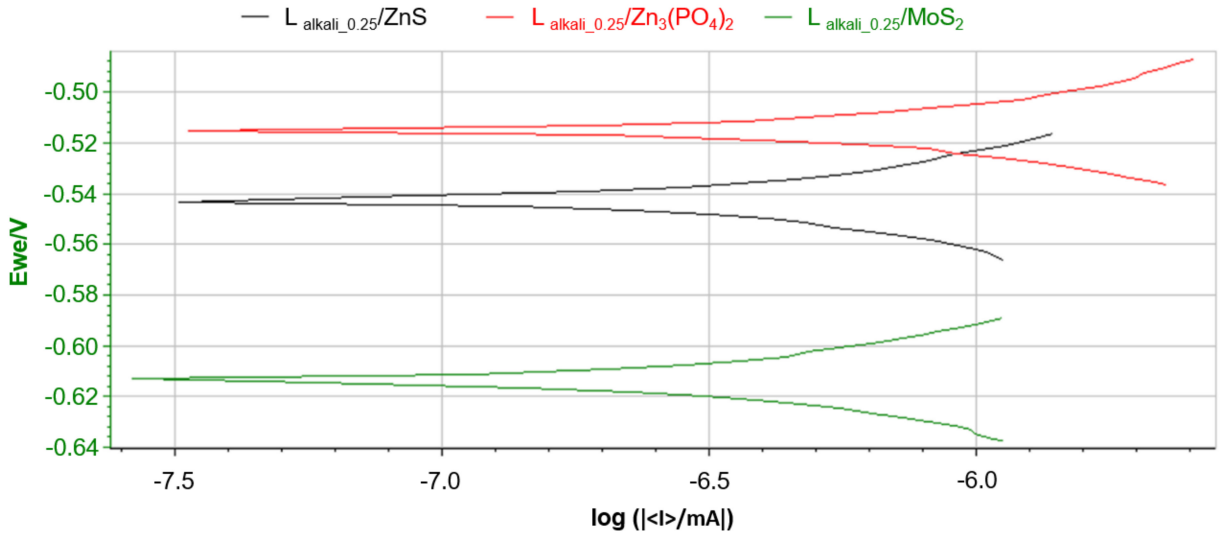

Figure 9. Tafel plots of the selected pigmented coatings: red line for $L_{\_alkali\_0.25}/Zn_3(PO_4)_2$, black line for $L_{\_alkali\_0.25}/ZnS$ and green line for $L_{\_alkali\_0.25}/MoS_2$.

The paint coatings from the latex $L_{acid\_0.25}$ and the reference latex L_{acid_0} containing ZnO and $ZnFe_2O_4$ achieved values one order of magnitude higher for their polarization resistances (from 1.0 to 4.2 MΩ) compared with the corresponding types of non-pigmented coatings. The pigmentation of these latices with $Zn_3(PO_4)_2$, ZnS, and MoS_2 pigments had an even more positive impact on the corrosion resistance of paint coatings, with increases of two orders of magnitude in their polarization resistance values (from 11 to 29 MΩ) compared with the corresponding types of non-pigmented coatings. The highest value of polarization resistance, 29 MΩ, was determined for the $L_{acid\_0.25}/MoS_2$ coating.

Comparable conclusions are valid for the latices synthesized at a 0.25 wt. % pyrrole dosage and the reference latices without polypyrrole in alkali form, where an identical trend of increased anticorrosive performance was observed. Even higher values of polarization resistance (from 13 to 30 MΩ) were achieved for these individual systems after alkalization compared with the corresponding types of systems before alkalization. The corrosion rate parameter decreased with increasing polarization resistance values. The highest value of polarization resistance, 30 MΩ, was determined for the latex coating $L_{alkali\_0.25}/MoS_2$.

As a result of the pigmentation of the synthesized latex binders with the incorporated polypyrrole components, the anticorrosion performance of these systems was increased when compared with non-pigmented systems. $Zn_3(PO_4)_2$ is a pigment which has been used commercially in coatings for decades, and its mechanisms of action have been described in detail [89]. The ZnS, ZnO, and MoS_2 pigments are characterized by their semiconductor nature, and the lamellar shape of the MoS_2 pigment particles contributes to the increase in adhesion-barrier resistance when this pigment is used in coatings. The semiconductor nature is also typical of the $ZnFe_2O_4$ pigment with its chemical mechanism of action [90].

These results clearly show that pigmentation has a positive effect on the corrosion resistance of the latex coatings studied. The selected pigments (ZnS and MoS_2) showed high compatibility with latex synthesized at a 0.25 wt. % pyrrole dosage. For these coating systems, the proven anticorrosion performance of the pigments (MoS_2 and ZnS) is combined with the anticorrosion performance of the binder itself, containing the electroactive polypyrrole component.

4. Conclusions

The research described in this paper aimed to synthesize and test polyacrylate latices containing electroactive composite polypyrrole-coated polyacrylate particles with a new laboratory protocol for producing stable, functional coating binders. The procedure using the "one-pot" synthesis strategy enabled not only the emulsion polymerization of acrylate monomers but also the oxidative polymerization of pyrrole to generate aqueous dispersion of chemically different submicron particles, namely polyacrylate and composite polypyrrole-coated polyacrylate. This technological procedure not only brings about environmental friendliness and time and energy savings to the production process but also offers the possibility of improving the quality and versatility of the latex binder. The chemical structure of polypyrrole synthesized during emulsion polymerization and the storage stability and physico-mechanical properties of the latices were evaluated. The protective barrier efficiency of non-pigmented coatings on steel substrate was evaluated using a cyclic corrosion test in a neutral salt mist atmosphere and using linear polarization. With this technique, the properties of prepared pigmented coatings were also studied. According to the findings, the following conclusions can be given:

- The polypyrrole component occurred in the prepared latices in a partly deprotonated yet conducting electroactive form.
- Latices synthesized using a 0.25 wt. % dosage of pyrrole reached sufficiently high zeta potential values, typical for stable colloidal systems, and showed favorable paint properties.
- Nonpigmented coatings cast from latices synthesized using a 0.25 wt. % dosage of pyrrole achieved higher anti-corrosion efficiency compared with the corresponding types of reference latices without the polypyrrole component.
- The ZnS and MoS_2 pigments showed compatibility with latices synthesized at a 0.25 wt. % dosage of pyrrole. For these paint coating systems, excellent anti-corrosion performance was demonstrated by the highest values of polarization resistance.

Author Contributions: Methodology, K.B., M.K., A.K., P.K., M.T., J.S., E.S. and J.M.; Validation, M.K., A.K., P.K., M.T., E.S., J.S. and J.M.; Formal analysis, J.M.; Investigation, K.B., M.K., A.K., P.K., M.T., J.S. and E.S.; Data curation, K.B., M.K. and A.K.; Writing—original draft, K.B. and J.M.; Writing—review & editing, K.B. and J.M.; Supervision, J.M.; Funding acquisition, M.K. and A.K. All authors have read and agreed to the published version of the manuscript.

Funding: This research received no external funding.

Institutional Review Board Statement: Not applicable.

Informed Consent Statement: Not applicable.

Data Availability Statement: Data are contained within the article.

Conflicts of Interest: The authors declare no conflict of interest.

References

1. Price, K.; Wu, W.; Wood, K.; Kong, S.; McCormick, A.; Francis, L. Stress development and film formation in multiphase composite latexes. *J. Coat. Technol. Res.* **2014**, *11*, 827–839. [CrossRef]
2. Li, X.; Wang, X.; Shen, Y.; Lai, X.; Wang, R.; Lv, H.; Fan, H. Synthesis and characterization of self-crosslinked polyurethane/polyacrylate composite emulsion based on carbonyl–hydrazide reaction. *J. Polym. Res.* **2013**, *20*, 270. [CrossRef]
3. Bhat, S.I.; Mobin, M.; Islam, S.; Zehra, S.; ul-Islam, S. Recent advances in anticorrosive coatings based on sustainable polymers: Challenges and perspectives. *Surf. Coat. Technol.* **2024**, *480*, 130596. [CrossRef]
4. Tian, X.; Lv, S.; Li, J.; Zhang, J.; Yu, L.; Liu, X.; Xin, X. Recent advancement in synthesis and modification of water-based acrylic emulsion and their application in water-based ink: A comprehensive review. *Prog. Org. Coat.* **2024**, *189*, 108320. [CrossRef]
5. Liang, C.; Feng, B.; Wang, S.; Zhao, B.; Xie, J.; Huang, G.; Zhu, L.; Hao, J. Differentiated emissions and secondary organic aerosol formation potential of organic vapor from industrial coatings in China. *J. Hazard. Mater.* **2024**, *466*, 133668. [CrossRef]
6. Ran, J.; Kioumourtzoglou, M.A.; Sun, S.; Han, L.; Zhao, S.; Zhu, W.; Li, J.; Tian, L. Source-specific volatile organic compounds and emergency hospital admissions for cardiorespiratory diseases. *Int. J. Environ. Res. Public Health* **2020**, *17*, 6210. [CrossRef]
7. Picchio, M.L.; Passeggi, M.C.G.; Barandiaran, J.; Gugliotta, L.M.; Minari, R.J. Waterborne acrylic-casein latexes as eco-friendly binders for coatings. *Prog. Org. Coat.* **2015**, *88*, 8–16. [CrossRef]
8. Mestach, D.; Twene, D. Acrylic dispersion for industrial with polymer-bound stabilizers. *Paint. Coat. Ind.* **2005**, *3*, 74–82.
9. Li, H.; Zhou, J.; Zhao, J.; Li, Y.; Kun, L. Synthesis of cellulose nanocrystals-armored fluorinated polyacrylate latexes via Pickering emulsion polymerization and their film properties. *Colloids Surf. B Biointerfaces* **2020**, *192*, 110071. [CrossRef]
10. Anderson, C.D.; Daniels, E.S. *Emulsion Polymerization and Latex Applications*; Smithers Rapra Publishing: Shropshire, UK, 2003; ISBN 1859573819.
11. Weldon, D.G. Acrylic latex coating. In *Failure Analysis of Paints and Coatings*; Wiley: Chichester, UK, 2009; pp. 92–95. ISBN 978-0-470-74466-6.
12. Zhang, X.; Chen, K.; Li, Z.; Zhang, Q.; Xu, C.; Chang, X.; Wen, S. Preparation of cross-linkable cationic polyacrylate latex and its film properties. *JCTR* **2023**, *21*, 341–354. [CrossRef]
13. Berce, S.; Skale, M.; Slemnik, M. Electrochemical impedance spectroscopy study of waterborne coatings film formation. *Prog. Org. Coat.* **2015**, *82*, 1–6. [CrossRef]
14. Beach, M.; Davey, T.; Subramanian, P.; Such, G. Self-healing organic coatings–Fundamental chemistry to commercial application. *Prog. Org. Coat.* **2023**, *183*, 107759. [CrossRef]
15. Elhalawany, N.; Saleeb, M.M.; Zahran, M.K. Novel anticorrosive emulsion-type paints containing organic/inorganic nano-hybrid particles. *Prog. Org. Coat.* **2014**, *77*, 548–556. [CrossRef]
16. Ashery, A.; Salem, M.A.; Farag, A.A.M. Optical and electrical performance of polypyrrole thin films and its hybrid junction applications. *Optik* **2018**, *172*, 302–310. [CrossRef]
17. Chitte, H.K.; Shinde, G.N.; Narendra, V.B.; Walunj, V.E. Synthesis of polypyrrole using ferric chloride ($FeCl_3$) as oxidant together with some dopants for use in gas sensors. *J. Sens. Technol.* **2011**, *1*, 47–56. [CrossRef]
18. Jain, A.; Nabeel, A.N.; Bhagwat, S.; Kumar, R.; Sharma, S.; Kozak, D.; Hunjet, A.; Kumar, A.; Singh, R. Fabrication of polypyrrole gas sensor for detection of NH_3 using an oxidizing agent and pyrrole combinations: Studies and characterizations. *Heliyon* **2023**, *9*, e17611. [CrossRef]
19. Sari, G.; Hafozah, M.A.E.; Manaf, A. Increased electrical conductivity of polypyrrole through emulsion polymerization assisted emulsifier synthesis. *IOP Conf. Ser. Mater. Sci. Eng.* **2019**, *553*, 012042. [CrossRef]
20. Prokeš, J.; Stejskal, J.; Omastová, M. Polyaniline, and polypyrrole—Two representatives of conducting polymers. *Chem. Listy* **2001**, *95*, 484–492.
21. Liu, G.; Hpu, F.; Wang, X.; Fang, B. Conductive Polymer and Nanoparticle-Promoted Polymer Hybrid Coatings for Metallic Bipolar Plates in Proton Membrane Exchange Water Electrolysis. *Appl. Sci.* **2023**, *13*, 1244. [CrossRef]
22. Sun, Y.; Hu, C.; Cui, J.; Shen, S.; Qiu, H.; Li, J. Electrodeposition of polypyrrole coatings doped by benzenesulfonic acid-modified graphene oxide on metallic bipolar plates. *Prog. Org. Coat* **2022**, *170*, 106995. [CrossRef]
23. Liu, S.; Pan, T.J.; Wang, R.F.; Yue, Y.; Shen, J. Anti-corrosion and conductivity of the electrodeposited graphene/polypyrrole composite coating for metallic bipolar plates. *Prog. Org. Coat* **2019**, *136*, 105237. [CrossRef]
24. Vernitskaya, T.V.; Efimov, O.N. Polypyrrole: A conducting polymer; its synthesis, properties, and applications. *Russ. Chem. Rev.* **1997**, *66*, 443–457. [CrossRef]
25. Ibrahim, F.A.; Khalaf, A.I.; Badr, M.M. Conductive polypyrrole: Synthesis, characterization, thermal, and electrical properties for different applications. *Phys. Scr.* **2024**, *99*, 065971. [CrossRef]
26. Liu, C.F.; Maruyama, T.; Yamamoto, T. Conductive blends of π-conjugated polymers and thermoplastic polymers in latex form. *Polym. J.* **1993**, *25*, 363–372. [CrossRef]
27. Omastová, M.; Micusik, M. Polypyrrole coating of inorganic and organic materials by chemical oxidative polymerisation. *Chem. Pap.* **2012**, *66*, 392–414. [CrossRef]
28. Mahmood, J.; Arsalani, N.; Naghash-Hamed, S.; Hanif, Z.; Geckeler, K.E. Preparation and characterization of hybrid polypyrrole nanoparticles as a conducting polymer with controllable size. *Sci. Rep.* **2024**, *14*, 11653. [CrossRef]

29. Tabačiarová, J.; Mičušík, M.; Fedorko, P.; Omastová, M. Study of polypyrrole aging by XPS, FTIR, and conductivity measurements. *Polym. Degrad. Stab.* **2015**, *120*, 392–401. [CrossRef]
30. Hao, L.; Dong, C.; Yu, D. Polypyrrole Derivatives: Preparation, Properties and Application. *Polymers* **2024**, *16*, 2233. [CrossRef]
31. Khadem, F.; Pishvaei, M.; Salami-Klajahi, M.; Najafi, F. Morphology control of conducting polypyrrole nanostructures via operational conditions in the emulsion polymerization. *J. Appl. Polym. Sci.* **2017**, *134*, 44697. [CrossRef]
32. Arunsawad, S.; Srikulkit, K.; Limpanart, S. Effect of surfactant on conductivity of Poly(pyrrole-co-formyl pyrrole) via Emulsion Polymerization. *J. Met. Mater. Miner.* **2014**, *24*, 759–765. [CrossRef]
33. Hoshina, Y.; Zaragoza-Contreras, E.A.; Farnood, R.; Kobayashi, T. Nanosized polypyrrole affected by surfactant agitation for emulsion polymerization. *Polym. Bull.* **2012**, *68*, 1689–1705. [CrossRef]
34. Wiersma, A.E.; vd Steeg, L.M.A.; Jongeling, T.J.M. Waterborne core-shell dispersions based on intrinsically conducting polymers for coating applications. *Synth. Met.* **1995**, *7*, 2269–2270. [CrossRef]
35. Morsi, S.M.M.; El-Aziz, M.A.; Morsi, R.M.M.; Hussain, A.I. Polypyrrole-coated latex particles as core/shell composites for anti-static coatings and energy storage applications. *JCTR* **2019**, *16*, 745–759. [CrossRef]
36. *ISO 706:2004*; Rubber Latex—Determination of Coagulum Content (Sieve Residue). International Organization for Standardization: Geneva, Switzerland, 2004.
37. Kolář, M.; Machotová, J.; Hájek, M.; Honzíček, J.; Hájek, T.; Podzimek, Š. Application of vegetable oil-based monomers in the synthesis of acrylic latexes via emulsion polymerization. *Coatings* **2023**, *13*, 262. [CrossRef]
38. Wu, Z.M.; Zhai, W.Z.; Song, P.F.; Wang, R.M. Silicylacrylate copolymer core-shell emulsion for humidity coatings. *Prog. Org. Coat.* **2014**, *77*, 1841–1847. [CrossRef]
39. He, L.; Liang, J.Z. Synthesis, modification and characterization of core-shell fluoroacrylate copolymer latexes. *J. Fluor. Chem.* **2008**, *129*, 590–597. [CrossRef]
40. *ISO 787-9:2019*; General Methods of Test for Pigments and Extenders, Part 9: Determination of pH Value of an Aqueous Suspension. International Organization for Standardization: Geneva, Switzerland, 2019.
41. Bin Razali, M.N.; Alkaf, A.A.; Zuhan, M.K.N.B. Formulation of water-based white colour paint from waste titanium dioxide. *Mater. Today Proc.* **2022**, *48*, 1905–1909. [CrossRef]
42. *ISO 2115:1996*; Plastics—Polymer Dispersions—Determination of White Point Temperature and Minimum Film-Forming Temperature. International Organization for Standardization: Geneva, Switzerland, 1996.
43. Machotová, J.; Zgoni, H.; Podzimek, S.; Svoboda, R.; Polarčik, J.; Šňupárek, J. Property study of structured self-crosslinking acrylic latex binder: Effect of molar mass and particle design. *Prog. Org. Coat.* **2017**, *111*, 258–266. [CrossRef]
44. Machotová, J.; Kalendová, A.; Steinerová, D.; Mácová, P.; Slang, S.; Šňupárek, J.; Vajdák, J. Water-resistant latex coatings: Tuning of properties by polymerizable surfactant, covalent crosslinking and nanostructured ZnO additive. *Coatings* **2021**, *11*, 347. [CrossRef]
45. Bhattacharjee, S. DLS and zeta potential—What they are and what they are not? *J. Control Release* **2016**, *235*, 337–351. [CrossRef]
46. Machotová, J.; Kalendová, A.; Voleská, M.; Steinerová, D.; Pejchalová, M.; Knotek, P.; Zárybnická, L. Waterborne hygienic coatings based on self-crosslinking acrylic latex with embedded inorganic nanoparticles: A comparison of nanostructured ZnO and MgO as antibacterial additives. *Prog. Org. Coat.* **2020**, *147*, 105704. [CrossRef]
47. Kumthekar, V.; Kolekar, S. Attributes of the latex emulsion processing and its role in morphology and performance in paints. *Prog. Org. Coat.* **2011**, *72*, 380–386. [CrossRef]
48. Steinerová, D.; Kalendová, A.; Machotová, J.; Knotek, P.; Humpolíček, P.; Vajdák, J.; Slang, S.; Krejčová, A.; Beneš, L.; Wolff-Fabris, F. Influence of Metal Oxide Nanoparticles as Antimicrobial Additives Embedded in Waterborne Coating Binders Based on Self-Crosslinking Acrylic Latex. *Coatings* **2022**, *12*, 1445. [CrossRef]
49. Bílková, E.; Sedlák, M.; Imramovský, A.; Chárová, P.; Knotek, P.; Benes, L. Prednisolone-α-cyclodextrin-star poly(ethylene glycol) polypseudorotaxane with delayed pH-sensitivity as a targeted drug delivery system. *Int. J. Pharm.* **2011**, *414*, 42. [CrossRef] [PubMed]
50. Wang, J.; Xu, H.; Battocchi, D.; Bierwagen, G. The determination of critical pigment volume concentration (CPVC) in organic coatings with fluorescence microscopy. *Prog. Org. Coat.* **2014**, *77*, 2147–2154. [CrossRef]
51. Lobnig, R.E.; Villaba, W.; Vogelsang, J.; Schmidt, R.; Zanger, P.; Soetemann, J. Development of a new experimental method to determine critical pigment–volume–concentrations using impedance spectroscopy. *Prog. Org. Coat.* **2006**, *55*, 363–374. [CrossRef]
52. *ISO 1514:2024*; Paints and Varnishes—Standard Panels for Testing. International Organization for Standardization: Geneva, Switzerland, 2024.
53. Kohl, M.; Alafid, F.; Boštíková, K.; Krejčová, A.; Slang, S.; Řezníček, D.; Hrdina, R.; Kalendová, A. Preparation and testing of anti-corrosion properties of new pigments containing structural units of melamine and magnesium cations (Mg_{2+}). *Coatings* **2023**, *13*, 1968. [CrossRef]
54. *ISO 2808:2019*; Paints and Varnishes—Determination of Film Thickness. International Organization for Standardization: Geneva, Switzerland, 2019.
55. *ISO 1522:2022*; Paints and Varnishes—Pendulum Damping Test. International Organization for Standardization: Geneva, Switzerland, 2022.
56. *ISO 2813:2014*; Paints and Varnishes—Determination of Gloss Value at 20°, 60° and 85°. International Organization for Standardization: Geneva, Switzerland, 2014.

57. *ISO 6272-1:2011*; Paints and Varnishes—Rapid-Deformation (Impact Resistance) Tests, Part 1: Falling-Weight Test, Large-Area Indenter. International Organization for Standardization: Geneva, Switzerland, 2011.
58. Goldschmidt, A.; Streitberger, H.J. *BASF Handbook on Basics of Coating Technology*; Vincentz Network: Hanover, Germany, 2007; pp. 345–393. ISBN 9783866303362.
59. *ISO 1520:2006*; Paints and Varnishes—Cupping Test. International Organization for Standardization: Geneva, Switzerland, 2006.
60. *ISO 1519:2011*; Paints and Varnishes—Bend Test (Cylindrical Mandrel). International Organization for Standardization: Geneva, Switzerland, 2011.
61. *ISO 2409:2020*; Paints and Varnishes—Cross-Cut Test. International Organization for Standardization: Geneva, Switzerland, 2020.
62. Do, J.; Cha, D.; Park, I.; Kwon, O.K.; Bae, J.; Park, J. Hydrothermal synthesis and application of adsorbent coating for ad-sorption chiller. *Prog. Org. Coat.* **2019**, *128*, 59–68. [CrossRef]
63. *ASTM D610-08*; Standard Practice for Evaluating Degree of Rusting on Painted Steel Surfaces. ASTM International: West Conshohocken, PA, USA, 2016.
64. *ASTM D714-02*; Standard Test Method for Evaluating Degree of Blistering of Paints. ASTM International: West Conshohocken, PA, USA, 2017.
65. *ISO 9227:2022*; Corrosion Tests in Artificial Atmospheres—Salt Spray Tests. International Organization for Standardization: Geneva, Switzerland, 2022.
66. *ISO 4628-8:2012*; Paints and Varnishes—Evaluation of Degradation of Coatings—Designation of Quantity and Size of Defects, and of Intensity of Uniform Changes in Appearance, Part 8: Assessment of Degree of Delamination and Corrosion Around a Scribe or Other Artificial Defect. International Organization for Standardization: Geneva, Switzerland, 2012.
67. De Freitas Cunha Lins, V.; de Andrade Reis, G.F.; de Araujo, C.R.; Matencio, T. Electrochemical impedance spectroscopy, and linear polarization applied to the evaluation of porosity of phosphate conversion coatings on electrogalvanized steels. *Appl. Surf. Sci.* **2006**, *253*, 2875–2884. [CrossRef]
68. Stejskal, J.; Trchová, M.; Morávková, Z.; Bober, P.; Kopecký, D.; Kopecká, J.; Watzlová, E.; Varga, M.; Prokeš, J. Polypyrrole salts and bases: Superior conductivity of nanotubes and their stability towards the loss of conductivity by deprotonation. *RSC Adv.* **2016**, *6*, 88382–88391. [CrossRef]
69. Pavithra, S.; Thejas, R.; Anil Rao, H.N.; Krishna, B.S.; Nagaraju, G. Preparation of polypyrrole by chemical oxidation: Applications for sensor studies. *Macromol. Res.* **2024**, *32*, 23–33. [CrossRef]
70. Blinova, N.V.; Stejskal, J.; Trchová, M.; Prokeš, J.; Omastová, M. Polyaniline and polypyrrole: A comparative study of the preparation. *Eur. Polym. J.* **2007**, *43*, 2331–2341. [CrossRef]
71. Kolthoff, I.M.; Miller, I.K. The chemistry of persulfate. I. The kinetics and mechanism of the decomposition of the persulfate ion in aqueous medium1. *JACS* **1951**, *73*, 3055–3059. [CrossRef]
72. Brooks, B.W.; Makanjuola, B.O. The rate of persulfate decomposition in the presence of polymer latices. *Die Makromol. Chem. Rapid Commun.* **1981**, *2*, 69–73. [CrossRef]
73. Gallardo, V.; Morales, M.E.; Ruiz, M.A.; Delgado, A.V. An experimental investigation of the stability of ethylcellulose latex: Correlation between zeta potential and sedimentation. *Eur. J. Pharm. Sci.* **2005**, *26*, 170–175. [CrossRef]
74. Müller, B.; Schackmann, M. *Coatings Formulation*; Lack in Vincentz GmbH and Company KG: Hannover, Germany, 2023.
75. Sakota, K.; Okaya, T. Electrolyte stability of carboxylated latexes prepared by several polymerization processes. *J. Appl. Polym. Sci.* **1977**, *21*, 1025–1034. [CrossRef]
76. Okubo, M.; Izumi, J.; Takekoh, R. Production of micron-sized monodispersed core/shell composite polymer particles by seeded dispersion polymerization. *Colloid. Polym. Sci.* **1999**, *277*, 875–880. [CrossRef]
77. Smolík, J.; Knotek, P.; Schwarz, J.; Černošková, E.; Kutálek, P.; Králová, V.; Tichý, L. Laser direct writing into PbO-Ga_2O_3 glassy system: Parameters influencing microlenses formation. *Appl. Surf. Sci.* **2021**, *540*, 148368. [CrossRef]
78. Capella, B.; Baschieri, P.; Frediani, C.; Miccoli, P.; Ascoli, C. Force-distance curves by AFM. *IEEE Eng. Med. Biol. Mag.* **1997**, *16*, 58. [CrossRef]
79. Hsieh, M.-T.; Endo, B.; Zhang, Y.; Bauer, J.; Valdevit, L. The mechanical response of cellular materials with spinodal topologies. *J. Mech. Phys. Solids* **2019**, *125*, 401–419. [CrossRef]
80. Blackley, D.C.; Blackley, D.C. Latex and paper. In *Polymer Latices: Science and Technology Volume 3: Applications of Latices*; Springer: Berlin/Heidelberg, Germany, 1997; pp. 434–473.
81. Machotova, J.; Podzimek, S.; Kvasnicka, P.; Zgoni, H.; Snuparek, J.; Cerny, M. Effect of molar mass on film-forming properties of self-crosslinking latexes based on structured acrylic microgels. *Prog. Org. Coat.* **2016**, *92*, 23–28. [CrossRef]
82. Anita, N.; Joany, R.M.; Dorothy, R.; Aslam, J.; Rajendran, S.; Subramania, A.; Singh, G.; Verma, C. Chapter 4—Linear polarization resistance (LPR) technique for corrosion measurements. In *Electrochemical and Analytical Techniques for Sustainable Corrosion Monitoring, Advances, Challenges and Opportunities*; Elsevier: Amsterdam, The Netherlands, 2023; pp. 59–80.
83. Sun, H.; Su, G.; Zhang, Y.; Ren, J.; Chen, X.; Hou, H.; Ding, Z.; Zhang, T.; Liu, W. First-principles modeling of the anodic and cathodic polarization to predict the corrosion behavior of Mg and its alloys. *Acta Mater.* **2023**, *244*, 118562. [CrossRef]
84. Rocchini, G. Corrosion rate monitoring by the linear polarization method. *Corros. Sci.* **1993**, *34*, 2031–2044. [CrossRef]
85. Zhang, X.L.; Jiang, Z.H.; Yao, Z.P.; Song, Y.; Wu, Z.D. Effects of scan rate on the potentiodynamic polarization curve obtained to determine the Tafel slopes and corrosion current density. *Corros. Sci.* **2009**, *51*, 581–587. [CrossRef]

86. Flitt, H.J.; Schweinsberg, D.P. Evaluation of corrosion rate from polarisation curves not exhibiting a Tafel region. *Corros. Sci.* **2005**, *47*, 3034–3052. [CrossRef]
87. Zhang, Y.; Die, J.; Li, F.; Li, H.; Tu, J.; Yu, X. Polypyrrole-Modified Molybdenum Disulfide Nanocomposite Epoxy Coating Inhibits Corrosion of Mild Steel. *Coatings* **2023**, *13*, 1046. [CrossRef]
88. Abdus Samad, U.; Alam, M.A.; Sherif, E.-S.M.; Alam, M.; Shaikh, H.; Alharthi, N.H.; Al-Zahrani, S.M. Synergistic Effect of Ag and ZnO Nanoparticles on Polypyrrole-Incorporated Epoxy/2pack Coatings and Their Corrosion Performances in Chloride Solutions. *Coatings* **2019**, *9*, 287. [CrossRef]
89. Hao, Y.; Liu, F.; Han, E.-H.; Anjum, S.; Xu, G. The mechanism of inhibition by zinc phosphate in an epoxy coating. *Corros. Sci.* **2013**, *69*, 77–86. [CrossRef]
90. Stejskal, J.; Trchová, M.; Brodinová, J.; Kalenda, P.; Fedorová, S.; Prokeš, J.; Zemek, J. Coating of zinc ferrite particles with a conducting polymer, polyaniline. *J. Colloid. Interface Sci.* **2006**, *298*, 87–93. [CrossRef]